Multi-User Wireless Information and Power Transfer in FBMC-Based IoT Networks

Sumaila Mahama, *Student Member, IEEE*, Derek Kwaku Pobi Asiedu, *Member, IEEE*, Yahya J. Harbi, *Member, IEEE*, Kyoung-Jae Lee, *Senior Member, IEEE*, David Grace, *Senior Member, IEEE* and Alister G. Burr, *Senior Member, IEEE*

In order to address the shortcomings of orthogonal frequency division multiplexing (OFDM) and extend the lifetime of energy-constrained Internet-of-Things (IoT) devices, the combination of filter bank multi-carrier (FBMC) and simultaneous wireless information and power transfer (SWIPT) is investigated in this paper. Specifically, a multi-user FBMC-based SWIPT system is proposed in which user nodes (UNs) have the capability for both energy harvesting (EH) and information decoding (ID) with the aid of separate antennas. A practical non-linear EH model, which considers the saturation effects of the EH circuit, is considered. The information receiver at both the UNs and base station (BS) adopts an iterative interference cancellation (IIC) receiver to cancel the intrinsic interference in the demodulated FBMC signal. A sum-rate maximization problem is solved to jointly optimize parameters such as time, power, and weight allocations. Sub-optimal schemes are proposed for comparison. Numerical results show that the optimal solution significantly outperforms the sub-optimal methods in terms of achievable sum-rate and amount of harvested energy. Moreover, the results show that the proposed algorithm converges within a few iterations.

***Index Terms*—Filter bank multi-carrier (FBMC), simultaneous wireless information and power transfer (SWIPT), time division multiple access (TDMA), sum-rate maximization, Internet-of-Things (IoT) networks.**

I. Introduction

In 5G new radio (NR), orthogonal frequency division multiplexing (OFDM) has been adopted as the modulation format for the physical layer (PHY) due to its many advantages, such as ease of implementation and backward compatibility with the existing 4G network. However, OFDM requires the grant-based synchronization procedure and the use of cyclic-prefix (CP) and guard band to maintain orthogonality between different sub-channels. For new 5G use cases, such as massive Machine-Type Communication (mMTC), the overhead and delay involved in the synchronization procedure can be significant due to the high connection density. Therefore, for such applications it is desirable to allow contention-based grant-free or asynchronous transmissions, in which each user node (UN) operates in a wake-up-and-transmit manner [1]. However, OFDM systems have been shown to perform poorly in asynchronous transmissions [2]. This is because OFDM suffers from poor out-of-band (OOB) emissions due to the use of rectangular filters, which can cause severe interference in asynchronous scenarios [3].

As a result, waveforms that are suitable for asynchronous access, such as filter bank multicarrier (FBMC), have been investigated for future wireless applications [4], [5]. FBMC employs well-localized prototype filters to improve the poor OOB leakage of OFDM, which reduces its sensitivity to asynchronous transmissions compared to OFDM. This makes FBMC a suitable alternative to OFDM in applications that require grant-free transmissions. By adopting FBMC, the strict synchronization procedure can be relaxed and CP overhead can be significantly reduced. Thus, improving the spectral efficiency compared to OFDM. In [1], the authors investigated the compatibility of FBMC with OFDM in a scenario where cellular users employing OFDM for synchronous communication coexist with mMTC users operating asynchronously using FBMC. The results showed that it is possible for OFDM-based cellular users to coexist with FBMC-based mMTC devices in future wireless networks.

A key challenge of FBMC systems is the lack of subcarrier orthogonality which causes intrinsic interference, i.e., intersymbol interference (ISI) and intercarrier interference (ICI). To eliminate ISI and ICI, offset QAM has been used in FBMC systems [6]. However, in FBMC-OQAM systems, orthogonality is achieved only in the real domain. The imaginary part of the signal causes intrinsic interference, which limits the direct implementation of conventional LTE-based schemes such as channel estimation and space-time block code (STBC) [7]. To resolve the problems in FBMC-OQAM, the transmission of complex QAM symbols in FBMC systems has been proposed [8], [9]. However, FBMC-QAM systems cannot guarantee complex domain orthogonality, resulting in high intrinsic interference.

Apart from the need for asynchronous access, it is essential for future mMTC networks to be self-sustaining [10]. In recent years, simultaneous wireless information and power transfer (SWIPT) has been recognized as a promising approach to provide device self-sustainability and prolong the battery life of energy-constrained wireless nodes [11], [12]. In SWIPT, a

The work of S. Mahama, D. Grace and A. G. Burr was supported by H2020-MSCA-SPOTLIGHT under grant number 722788. K.-J. Lee and D. K. P Asiedu's work was supported in part by the Institute for Information and Communications Technology Promotion through Korea Government (MSIT) under Grant 2018-0-00812 (IoT Wireless Powered Cognitive Radio Communications With User-Centric Distributed Massive MIMO Systems).

S. Mahama, D. Grace, and A. G. Burr are with the Department of Electronic Engineering, University of York, York, United Kingdom (email: sumaila.mahama@york.ac.uk; david.grace@york.ac.uk; alister.burr@york.ac.uk)

Derek. K. P. Asiedu and K.-J. are with the Department of Electronics and Control Engineering, Hanbat National University, Daejeon 34158, South Korea (email: kwakupobi@gmail.com; kyoungjae@hanbat.ac.kr)

Yahya J. Harbi is with the University of Kufa, Najaf, Iraq (email: yahyaj.harbi@uokufa.edu.iq)

Corresponding author: Sumaila Mahama (sumaila.mahama@york.ac.uk)

receiver node can harvest energy and decode information from the received radio frequency (RF) signal by employing either the separated receiver mode or co-located receiver mode [13]. In the separated receiver mode, separate receivers are used for information decoding (ID) and energy harvesting (EH). Thus, each receiver can have a dedicated antenna without the need to split the received signal. In the co-located receiver mode, on the other hand, a single receiver simultaneously performs ID and EH. The received signal is split into two portions for ID and EH by either time switching (TS) or power splitting (PS) [14]. Most early works in SWIPT assumed a linear EH model. However, practical EH devices consist of a rectifier circuit with diodes and transistors which imposes a non-linear behaviour on the EH circuit. Thus, non-linear EH models have been implemented for SWIPT recently [13], [15].

Dealing with the intrinsic interference caused by the loss of orthogonality is a key design requirement in FBMC-QAM systems. Unlike traditional wireless communications, in which the interference is treated as an undesired signal, it can be exploited as a useful signal for wireless EH in SWIPT systems [16]. By harnessing the benefits of FBMC-QAM and SWIPT, billions of IoT devices can be effectively connected and powered anywhere, any time.

A. Related Work

In recent years, a lot of research has been conducted to evaluate the performance of SWIPT in IoT networks. Most of the research at the physical layer has considered the combination of SWIPT with techniques such as cooperative communications, full-duplex and multicarrier waveforms. Asiedu *et al.* [12] studied a multi-hop decode-and-forward (DF) SWIPT system for IoT networks, and investigated two optimization problems with the aim of finding the optimal PS ratio to optimize the source transmit power and the achievable rate. [17] studied SWIPT for IoT sensor networks in which multiple transmitter-receiver pairs exchange information and energy by employing PS at the receiver node. The objective of [17] is to minimize the total transmit power by optimizing the message configurations, hybrid beamforming vectors, and PS ratio at the receiver nodes.

The performance of SWIPT in multicarrier waveforms has also been investigated in the literature [18]–[20]. In [18] a multi-user OFDM-based SWIPT system is investigated, in which two multiple access and EH schemes are implemented: (i) time division multiple access (TDMA) transmission with a TS-based receiver and (ii) orthogonal frequency division multiple access (OFDMA) transmission with a PS-based receiver. [19] proposed an OFDM-based SWIPT system in which the received signal is partitioned into two subcarriers groups: one group for ID and the other group for EH. Moreover, a joint subcarrier and power allocation problem is derived to maximize the harvested energy. A similar model is presented in [20], where the goal is to maximize the users' sum-rate by optimizing the channel allocation and power allocation. Because the received signal is separated into two groups for ID and EH, neither PS nor TS is needed at the receiver.

Majority of the existing work on SWIPT in multicarrier waveforms are based on OFDM. However, as mentioned above, OFDM does not meet all the requirements of future IoT applications, especially the need for a huge connection density and asynchronous access [1]. For such applications, non-orthogonal waveforms have been shown to perform better than OFDM [5]. To harness the advantages of SWIPT and non-orthogonal waveforms, the combination of generalized frequency division multiplexing (GFDM) and SWIPT has been investigated recently [21]–[23]. In [21], a GFDM-based cooperative relay system is proposed to improve the quality of experience and extend users' battery life at the edge of a cell. A joint subcarrier and subsymbol allocation for a multi-user SWIPT GFDM system is studied in [22], in which a sum-rate maximization problem is solved to optimize the sub-block allocation, power allocation, and PS ratio. The authors in [23] extended the SWIPT model in [21] to a GFDM-based amplify-and-forward (AF) system and derived an analytical expression for the bit error rate (BER).

B. Contribution

Motivated by the advantages of FBMC[1] systems over conventional OFDM, i.e., high spectral efficiency and suitability for asynchronous access, this paper focuses on the combination of FBMC and SWIPT for future IoT applications by exploiting the intrinsic interference in FBMC as a source of RF energy. The suitability of FBMC for asynchronous transmissions will enable the implementation of grant-free random access at the UNs, which can reduce the synchronization overhead and delay incurred in a typical OFDM-based system. Furthermore, in future wireless networks, an FBMC-based IoT network can coexist[2] with an OFDM-based cellular network to increase the overall system throughput and avoid the leakage interference involved in asynchronous communication in OFDM [1].

Specifically, a multi-user FBMC-based IoT network is considered, in which a single antenna base station (BS) transmits signals to multiple UNs in the downlink (DL) and receives signals from the UNs in the uplink (UL). Each UN can decode information and harvest energy from the received. For the SWIPT implementation, the separate receiver model with separate antennas for the energy and information receivers is considered. Thus, there is no need for TS or PS. The energy receiver is a combination of the antenna for RF energy reception and a rectifier to convert the received RF signal to DC. Moreover, unlike [22], a non-linear energy harvesting model, which is more practical, is adopted in this paper. In order to remove the intrinsic interference in FBMC an iterative interference cancellation (IIC) receiver is employed for the information decoding at both the BS and UN [24]–[26].

It was shown in [27] that because the prototype filters used in FBMC systems are well-localized in frequency domain, even-numbered subcarriers causes negligible interference to other even-numbered subcarriers i.e., only adjacent (even and odd-numbered) subcarriers interfere with each other. Therefore, following the work in [19], the DL signal is partitioned into even and odd-numbered groups where modulated data is

[1]In the sequel, we refer to FBMC-QAM simply as FBMC

[2]The coexist of FBMC-based SWIPT UNs with OFDM-based cellular users is an interesting future topic which is beyond the scope of this paper.

transmitted only on even-numbered sub-carriers[3]. The advantage of this is twofold: (i) by sampling only even-numbered sub-carriers for ID, the ICI level at the UN is significantly reduced, (ii) with reduced ICI, the complexity of the iterative receiver at the UN can also be reduced, which reduces the amount of power consumed by the IIC processing at each UN. Moreover, with a dedicated antenna, the energy receiver can harvest energy from both even and odd-numbered subcarriers. The harvested energy in the DL is then either used to support the UL transmission of the UNs or stored in a battery for the operations of the information receiver. Since the BS has a constant power supply and higher processing capacity for information processing, both even and odd-numbered subcarriers carry modulated data in the UL phase. The main contributions of this work are highlighted as follows:

- This paper investigates a multi-user FBMC-based SWIPT system in which no TS or PS is needed at the SWIPT receiver. A non-linear EH model is adopted to verify the practicality of the proposed model. The proposed system can provide network self-sustainability, improved spectral efficiency and suitability for asynchronous transmissions.
- An IIC receiver is implemented to cancel the intrinsic interference at the information receiver of both the UN and the BS.
- A weighted sum-rate (WSR) maximization problem is formulated with the aim of optimizing the weight allocation, time allocation, and power allocation of each UN under the total DL transmit power and EH constraints. To effectively solve the WSR problem, it is converted to an equivalent weighted minimum mean squared error (WMMSE) problem, which is then converted to two subproblems: (i) time and weight resource allocation problem and (ii) power resource allocation problem.
- The power allocation problem is found to be non-convex. Thus, an iterative optimization algorithm is proposed using closed-form solutions derived for the DL and UL power allocation. The time and weight allocation problem, on the other hand, is shown to be a convex problem. Therefore, closed-form expressions are derived for time and weight allocations in both DL and UL. The results show that equal time and weight allocations are optimal in the proposed model.
- A joint resource allocation algorithm is proposed to combine the solutions of the time and weight allocation problem and the power allocation problem. This algorithm is used to find the maximum WSR using the optimal resources from the two subproblems.
- A centralized approach is adopted such that the resource allocation computation is implemented at the BS. This is because the BS can obtain a global channel state information (CSI), has a bigger processing capacity and is supplied by a constant power source. Adopting a centralized approach reduces the computational burden and power consumption at the UN.

[3]This assumption follows from the fact that in many IoT applications the amount of downlink data received is very small compared to the uplink transmission.

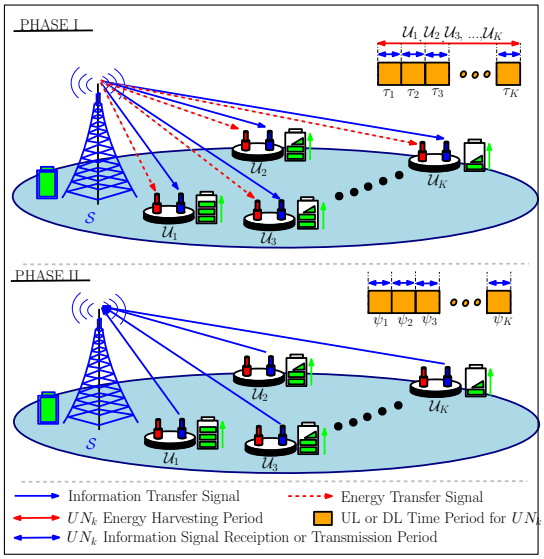

Fig. 1: Multi-user FBMC-QAM system model with separate antenna SWIPT architecture.

C. Organization

The remainder of the paper is organized as follows: In Section II, the proposed FBMC-based SWIPT system model and the problem formulation are described. The optimization solutions and algorithms are presented in Section III. Simulation results and complexity analysis of the proposed model are presented in Section IV. Finally, concluding remarks are provided in Section V.

II. System Model and Problem Formulation

In this section, the details of the proposed multi-user FBMC-based SWIPT system is discussed. The proposed system, shown in Fig. 1, consists of a single antenna BS and K UNs. Each UN has two antennas: one dedicated to information reception and transmission, and the other dedicated to energy reception. The UNs are scheduled to transmit and receive via TDMA.

A. Downlink Phase

In the DL phase, all UNs undertake EH and ID as shown in Fig. 1. It is shown in [27] that data on even-numbered subcarriers causes negligible interference to other even-numbered subcarriers. This is because FBMC systems employ prototype filters that are well-localized in the frequency domain which limits OOB leakage to adjacent subcarriers. Therefore, in order to reduce the level of intrinsic interference at the UN, QAM modulated data is inserted only on even-numbered subcarriers in the DL. With reduced interference at the UN, the complexity and power consumption of the information receiver can also be reduced. Under this setup, the n-th transmitted symbol vector from the BS to the k-th UN during its assigned time slot τ_k is given as

$$\mathbf{x}_{n,k}^{dl} = \mathbf{G}_{n,k}\mathbf{\Phi}\mathbf{a}_{n,k}^{dl} \tag{1}$$

where $\mathbf{x}_{n,k}^{dl} = [x_{0,n}^k, x_{1,n}^k, \ldots, x_{L-1,n}^k]$ is the vector of the transmitted signal, $L = O \times M$ with O as the overlapping

factor of the prototype filter, $\mathbf{\Phi}$ is the $M \times M$ inverse fast Fourier transform (IFFT) matrix with entries on the i-th row and j-th column given as $\sqrt{1/M}\exp(\sqrt{-1}\frac{2\pi ij}{M})$, M is the total number of subcarriers and $\mathbf{a}_{n,k}^{dl}$ represents the vector of transmitted data, given as

$$\mathbf{a}_{n,k}^{dl} = \begin{cases} a_{n,m}^{e,dl}, & \text{for } m \in \{0, 2, \ldots, M-2\} \\ 0, & \text{for } m \in \{1, 3, \ldots, M-1\} \end{cases} \tag{2}$$

$\mathbf{G}_{n,k}$ represents the $L \times M$ prototype filter matrix whose entry on the l-th diagonal is given as

$$g_{n,k}[l] = g[l - nM] \tag{3}$$

where $g[i]$ is the prototype filter coefficient [27]. Note that the PHYDYAS prototype filter presented in [28] is used for the per subcarrier filtering in this paper.

1) Information Receiver

At the information receiver, the received signal is first filtered, down-sampled and then passed through the FFT block. The resulting signal after the filtering operation is represented as

$$\begin{aligned} \mathbf{y}_{n,k}^{ID,dl} &= \mathbf{G}_{n,k}^H \mathbf{H}_k^{dl} \mathbf{x}_{n,k}^{dl} + \mathbf{G}_{n,k}^H \mathbf{z}_k^{dl} \\ &= \mathbf{G}_{n,k}^H \mathbf{H}_k^{dl} \mathbf{G}_{n,k} \mathbf{\Phi} \mathbf{a}_{n,k}^{dl} + \mathbf{G}_{n,k}^H \mathbf{z}_k^{dl} \\ &= \tilde{\mathbf{H}}_k^{dl} \mathbf{a}_{n,k}^{dl} + \mathbf{G}_{n,k}^H \mathbf{z}_k^{dl} \end{aligned} \tag{4}$$

where $\tilde{\mathbf{H}}_k^{dl} = \mathbf{G}_{n,k}^H \mathbf{H}_k^{dl} \mathbf{G}_{n,k} \mathbf{\Phi}$, $\mathbf{z}_k^{dl}$ is the $L \times 1$ additive white Gaussian noise (AWGN) vector at UN$_k$ and $\mathbf{H}_k^{dl}$ is the $L \times L$ multipath fading channel matrix between the BS and UN$_k$. The entry on the l-th diagonal of $\mathbf{H}_k^{dl}$ represents the complex channel gain of the l-th subchannel of UN$_k$ and can be modelled as [29]

$$h_{k,l} = \sqrt{A}\left(\frac{\tilde{d}}{d_k}\right)^{\frac{\kappa}{2}} \sqrt{\mathrm{g}_t \mathrm{g}_r} \exp\left(j2\pi \frac{d_k}{\lambda}\right) \tag{5}$$

where d_k is the distance between the BS and UN$_k$, $\tilde{d}$ is the reference distance for the path loss, A is the attenuation at the reference distance, κ is the path loss exponent, g_t is the BS antenna gain and g_r is the UN antenna gain. Also, λ represents the wavelength of the RF signal with frequency f_c.

The frequency domain signal vector after down-sampling and FFT is given as

$$\begin{aligned} \mathbf{y}_{n,k}^{dl} &= \mathbf{\Phi}^H \mathbf{y}_{n,k}^{ID,dl} \\ &= \mathbf{\Phi}^H \tilde{\mathbf{H}}_k^{dl} \mathbf{a}_{n,k}^{dl} + \mathbf{\Phi}^H \mathbf{G}_{n,k}^H \mathbf{z}_k^{dl} \\ &= \hat{\mathbf{H}}_k^{dl} \mathbf{a}_{n,k}^{dl} + \tilde{\mathbf{z}}_k^{dl} \end{aligned} \tag{6}$$

where $\hat{\mathbf{H}}_k^{dl} = \mathbf{\Phi}^H \tilde{\mathbf{H}}_k^{dl}$ is the $M \times M$ down-sampled effective channel matrix and $\tilde{\mathbf{z}}_k^{dl} = \mathbf{\Phi}^H \mathbf{G}_{n,k}^H \mathbf{z}_k^{dl}$ is the $M \times 1$ effective noise vector. As mentioned above, modulated data is inserted only on even-numbered subcarriers in the DL phase. Therefore, the sampled received signal on even-numbered subcarriers of the k-th UN can be expressed as

$$\mathbf{y}_{n,k}^{e,dl} = \hat{\mathbf{H}}_k^{e,dl} \mathbf{a}_{n,k}^{e,dl} + \tilde{\mathbf{z}}_k^{dl}, \tag{7}$$

where $\mathbf{a}_{n,k}^{e,dl} = [a_{n,0}^{e,dl}, a_{n,2}^{e,dl}, \ldots, a_{n,M-2}^{e,dl}]$ represents the data on even-numbered subcarriers and $\hat{\mathbf{H}}_k^{e,dl}$ is the corresponding $M/2 \times M/2$ effective channel matrix. By getting rid of the odd-numbered subcarriers, we can assume negligible ICI between subcarriers due to the low OOB emission performance of FBMC. This implies that UN$_k$ is only affected by ISI. Thus, the even-numbered demodulated signal associated to the m-th subcarrier and the n-th symbol for UN$_k$ is given as

$$r_{m,n,k}^{dl} = \hat{h}_{m,n,k}^{e,dl} a_{m,n}^{e,dl} + \underbrace{\sum_{n' \neq n} \sum_{m'=0}^{M} \hat{h}_{m',n',k}^{e,dl} a_{m',n'}^{e,dl}}_{I_{ISI}^{dl}} + \tilde{z}_k^{dl}. \tag{8}$$

where $\hat{h}_{m,n,k}^{e,dl}$ is the m-th diagonal element of $\hat{\mathbf{H}}_k^{e,dl}$.

To eliminate the ISI term in (8), an IIC receiver is implemented as shown in Algorithm 1 in Section III. Without loss of generality, it is assumed that the receiver undergoes enough IIC iterations to completely remove the ISI term in (8). This assumption has been made in order to obtain insight regarding the optimization of the resource allocation in the energy harvesting and data transmission of the proposed scheme. Moreover, with the reduced intrinsic interference at the UN, fewer number of IIC iterations are required to remove the ISI term in (8). As shown in [3], the IIC algorithm is capable of removing the intrinsic interference with a few iterations. We note that the extension to the case with residual interference after IIC is an important direction for future research[4]. Thus, the demodulated signal after the last IIC iteration can be expressed as

$$\hat{r}_{m,n,k}^{dl} = \hat{h}_{m,n,k}^{dl} a_{m,n,k}^{e,dl} + \tilde{z}_k^{dl}. \tag{9}$$

The effective signal-to-noise ratio (SNR) of UN$_k$ is calculated as the ratio of the signal power and the effective noise power. From (7), the power of the processed noise can be calculated as

$$\begin{aligned} \mathbb{E}[(\tilde{\mathbf{z}}_{n,k}^{dl})(\tilde{\mathbf{z}}_{n,k}^{dl})^H] &= \mathbb{E}[\mathbf{\Phi}^H \mathbf{G}_{n,k}^H (\mathbf{z}_k^{dl})(\mathbf{z}_k^{dl})^H \mathbf{G}_{n,k} \mathbf{\Phi}] \\ &= \mathbf{G}_{n,k}^H \mathbb{E}[(\mathbf{z}_k^{dl})(\mathbf{z}_k^{dl})^H] \mathbf{G}_{n,k} \\ &= \mathbf{G} \sigma_{z_k^{dl}}^2 \end{aligned} \tag{10}$$

where $\mathbf{G} = \mathbf{G}_{n,k}^H \mathbf{G}_{n,k}$ and $\sigma_{z_k^{dl}}^2$ represents the noise variance. Therefore, for the n-th symbol and m-th subcarrier of UN$_k$ the effective noise power, $\sigma_k^2 = g_{m,n,k} \sigma_{z_k^{dl}}^2$ is Gaussian. The corresponding SNR for UN$_k$ is defined as

$$SNR_{m,n,k}^{dl} = \frac{|\hat{h}_{m,n,k}^{dl}|^2 P_{m,n,k}^{dl}}{\sigma_k^2}, \tag{11}$$

where $P_{m,n,k}^{dl}$ is the power allocated to UN$_k$ in the DL. Therefore, the DL data rate of UN$_k$ for the time period τ_k is given by

$$R_k^{dl} = \alpha \tau_k T \sum_{n=1}^{N} \sum_{m=1}^{M} \log_2(1 + SNR_{m,n,k}^{dl}). \tag{12}$$

where N represents the number of FBMC symbols, T denote the total transmission time, and α is the time allocated for DL communication.

[4]Please refer to our work in [3] for an analysis of how many iterations is required to remove the interference below the error floor.

2) Energy Receiver

As mentioned above, each UN is equipped with a separate antenna for EH, which implies that each UN can harvest energy from all sub-carriers in every DL time slot. At the EH receiver, the contribution of noise is assumed to be negligible. Therefore, the received signal at the EH receiver of UN_k is given as

$$\begin{aligned}\mathbf{y}_{n,k}^{EH,dl} &= \mathbf{H}_k^{dl}\mathbf{x}_{n,k}^{dl} \\ &= \mathbf{H}_k^{dl}\mathbf{G}_{n,k}\mathbf{\Phi}\mathbf{a}_{n,k}^{dl} \\ &= \bar{\mathbf{H}}_k^{dl}\mathbf{a}_{n,k}^{dl}\end{aligned} \tag{13}$$

where $\bar{\mathbf{H}}_k^{dl} = \mathbf{H}_k^{dl}\mathbf{G}_{n,k}\mathbf{\Phi}$. Considering the linear EH model, the total harvested power by UN_k is given as

$$\begin{aligned}P_k^{linear} &= \frac{\alpha\beta_k}{(1-\alpha)\psi_k}\sum_{j=1}^{K}\tau_j\sum_{n=1}^{N}\sum_{m=1}^{M}|\bar{h}_{m,n,j}^{dl}|^2 P_{m,n,j}^{dl} \\ &= \frac{\alpha\beta_k}{(1-\alpha)\psi_k}\gamma_{m,n,j}^{dl}\end{aligned} \tag{14}$$

where β_k denotes the energy conversion efficiency in the linear region of the EH circuit, ψ_k is the UL transmission time of UN_k, $\bar{h}_{m,n,j}$ represents the diagonal entries of $\bar{\mathbf{H}}_k^{dl}$ and $\gamma_{m,n,j}^{dl} = \sum_{j=1}^{K}\tau_j\sum_{n=1}^{N}\sum_{m=1}^{M}|\bar{h}_{m,n,j}^{dl}|^2 P_{m,n,j}^{dl}$.

The linear EH model is employed in the literature due to its relatively simple implementation. However, it does not capture the non-linear behaviour of the rectifier circuit. To tackle the problem with the linear EH model, the practical EH model in [30] and [15], which uses a non-linear function to model the harvested power, is considered in this paper. By adopting this model, the non-linear harvested power of UN_k can be expressed as

$$P_k = \begin{cases}\Delta_k\gamma_{m,n,j}^{dl}, & \text{for } \gamma_{m,n,j}^{dl} \le P_{th} \\ \Delta_k P_{th}, & \gamma_{m,n,j}^{dl} > P_{th}\end{cases} \tag{15}$$

where $\Delta_k = \frac{\alpha\beta_k}{(1-\alpha)\psi_k}$ and P_{th} is the saturation threshold power of the EH receiver. During the UL time slot of UN_k, ψ_k, the UL transmit power is $P_k^{ul} = P_k$. Furthermore, each user is capable of harvesting energy during all time slots due to their dedicated energy antenna. The energy harvested in other time slots is stored in a battery and the information receiver draws power from the battery for its processing, e.g. IIC algorithm. While the additional processing required for IIC may consume some of the power harvested, there are many applications of IoT networks where the downlink data required to be detected at a UN is very small, and hence negligible compared to the total energy harvested.

B. Uplink Phase

Now, consider the multiple access UL communication between the BS and UNs. Since the BS has a higher processing capacity, it is assumed that modulated data is transmitted on both even and odd subcarriers in the UL. This is a practical assumption because in most IoT applications UNs will collect data and transmit to a BS, resulting in a higher data rate requirement on the UL compared to the DL. During time slot ψ_k, the n-th transmit symbol vector of UN_k is given as

$$\mathbf{x}_{n,k}^{ul} = \mathbf{G}_{n,k}\mathbf{\Phi}\mathbf{a}_{n,k}^{ul} \tag{16}$$

Similar to the DL phase, the received signal at the BS is filtered, down-sampled and converted to the frequency domain using the FFT operation. The signal at the output of the receive filter is expressed as

$$\begin{aligned}\mathbf{y}_{n,k}^{ID,ul} &= \mathbf{G}_{n,k}^H\mathbf{H}_k^{ul}\mathbf{x}_{n,k}^{ul} + \mathbf{G}_{n,k}^H\mathbf{z}^{ul} \\ &= \mathbf{G}_{n,k}^H\mathbf{H}_k^{ul}\mathbf{G}_{n,k}\mathbf{\Phi}_k\mathbf{a}_{n,k}^{ul} + \mathbf{G}_{n,k}^H\mathbf{z}^{ul} \\ &= \tilde{\mathbf{H}}_k^{ul}\mathbf{a}_{n,k}^{ul} + \mathbf{G}_{n,k}^H\mathbf{z}^{ul}.\end{aligned} \tag{17}$$

where $\tilde{\mathbf{H}}_k^{ul} = \mathbf{G}_{n,k}^H\mathbf{H}_k^{ul}\mathbf{G}_{n,k}\mathbf{\Phi}$, $\mathbf{z}^{ul}$ is the $L\times 1$ AWGN vector and $\mathbf{H}_k^{ul}$ is the $L\times L$ multipath fading channel matrix between UN_k and the BS. After down-sampling and FFT the frequency domain signal vector for UN_k is given as

$$\begin{aligned}\mathbf{y}_{n,k}^{ul} &= \mathbf{\Phi}^H\mathbf{y}_{n,k}^{ID,ul} \\ &= \mathbf{\Phi}^H\tilde{\mathbf{H}}_k^{ul}\mathbf{a}_{n,k}^{ul} + \mathbf{\Phi}^H\mathbf{G}_{n,k}^H\mathbf{z}^{ul} \\ &= \hat{\mathbf{H}}_k^{ul}\mathbf{a}_{n,k}^{ul} + \tilde{\mathbf{z}}^{ul}\end{aligned} \tag{18}$$

where $\hat{\mathbf{H}}_k^{ul} = \mathbf{\Phi}^H\tilde{\mathbf{H}}_k^{ul}$ and $\tilde{\mathbf{z}}^{ul} = \mathbf{\Phi}_k^H\mathbf{G}_{n,k}^H\mathbf{z}^{ul}$. Note that, unlike the UNs, the BS suffer from both ICI and ISI. Therefore, the demodulated signal associated with the m-th subcarrier and the n-th symbol of UN_k is given as

$$\begin{aligned}r_{m,n,k}^{ul} = \hat{h}_{m,n,k}^{ul}a_{m,n}^{ul} + \underbrace{\sum_{n'\neq n}\sum_{m'=0}^{M}\hat{h}_{m',n',k}^{ul}a_{m',n'}^{ul}}_{I_{ISI}^{ul}} \\ + \underbrace{\sum_{m'\neq m}\hat{h}_{m',n,k}^{ul}a_{m',n}^{ul}}_{I_{ICI}^{ul}} + \tilde{z}^{ul}\end{aligned} \tag{19}$$

where $\hat{h}_{m,n,k}^{ul}$ is the m-th diagonal element of $\hat{\mathbf{H}}_k^{ul}$. As in the DL case, the ICI and ISI terms are estimated and removed by applying a fixed number of IIC iterations at the BS. Assuming perfect cancellation of the intrinsic interference after IIC, the resulting processed signal is given as

$$\hat{r}_{m,n,k}^{ul} = \hat{h}_{m,n,k}^{ul}a_{m,n,k}^{ul} + \tilde{z}^{ul}. \tag{20}$$

The effective noise power, σ^2, is calculated as shown in (10). Thus, the SNR and rate at the BS from the received signal of UN_k can be represented as

$$SNR_{m,n,k}^{ul} = \frac{|\hat{h}_{m,n,k}^{ul}|^2 P_{m,n,k}^{ul}}{\sigma^2} \quad \text{and} \tag{21}$$

$$R_k^{ul} = (1-\alpha)\psi_k T\sum_{n=1}^{N}\sum_{m=1}^{M}\log_2(1+SNR_{m,n,k}^{ul}), \tag{22}$$

respectively.

C. Problem Formulation

Consider the fact that, at each transmit node (UNs or BS), a maximum power threshold is set on the transmit power and that each node's transmission is restricted to its allocated time slot. Under these constraints, we aim to maximize the UL-DL WSR of each UN. Mathematically, the UL-DL WSR

maximization problem for the proposed FBMC-based SWIPT system is formulated as

$$\begin{aligned} P(1): \underset{L_g}{\text{maximize}} \quad & \sum_{k=1}^{K}\left[\omega_k^{dl}R_k^{dl}+\omega_k^{ul}R_k^{ul}\right] \\ \text{subject to} \quad & \sum_{m=1}^{M}\sum_{n=1}^{N}P_{m,n,k}^{dl}\le P_{0,max}^{dl},\ \omega_k^{dl}\ge 0, \\ & \sum_{m=1}^{M}\sum_{n=1}^{N}P_{m,n,k}^{ul}\le P_k^{ul}-P_c,\ \omega_k^{ul}\ge 0, \\ & \alpha\sum_{k=1}^{K}\tau_k+(1-\alpha)\sum_{k=1}^{K}\psi_k=T, \end{aligned} \tag{23}$$

where $P_{0,max}^{dl}$ is the maximum transmit power at the BS and P_c is the power consumed by UN$_k$ for information processing. ω_k^{dl} and ω_k^{ul} are the DL and UL weights for UN$_k$. $L_g = [\alpha, \{P_{m,n,k}^{dl}\}, \{P_{m,n,k}^{ul}\}, \{\psi_k\}, \{\tau_k\}, \{\omega_k^{dl}\}, \{\omega_k^{ul}\}]$. To reduce the complexity involved in solving problem $P(1)$, it is converted to an equivalent WMMSE minimization problem [31]. The WSR to WMMSE conversion steps are presented in Appendix A. The WMMSE problem is expressed as

$$\begin{aligned} P(2): \underset{L_g}{\text{minimize}} \quad & \sum_{k=1}^{K}\sum_{n=1}^{N}\sum_{m=1}^{M}\left[\bar{\omega}_k^{dl}e_{m,n,k}^{dl}+\bar{\omega}_k^{ul}e_{m,n,k}^{ul}\right] \\ \text{subject to} \quad & \sum_{n=1}^{N}\sum_{m=1}^{M}P_{m,n,k}^{dl}\le P_{0,max}^{dl},\ \bar{\omega}_k^{dl}\ge 0, \\ & \sum_{k=1}^{K}\sum_{n=1}^{N}\sum_{m=1}^{M}P_{m,n,k}^{ul}\le P_k^{ul}-P_c,\ \bar{\omega}_k^{ul}\ge 0 \\ & \alpha\sum_{k=1}^{K}\tau_k+(1-\alpha)\sum_{k=1}^{K}\psi_k=T, \end{aligned} \tag{24}$$

where $\bar{\omega}_k^{dl}$ and $\bar{\omega}_k^{ul}$ are the WMMSE weights for UN$_k$ on the DL and UL, respectively. Also,

$$e_{m,n,k}^{dl}=\frac{\sigma_{z^{dl}}^2}{|\hat{h}_{m,n,k}^{dl}|^2P_{m,n,k}^{dl}+\sigma_k^2} \tag{25}$$

and

$$e_{m,n,k}^{ul}=\frac{\sigma_{z^{ul}}^2}{|\hat{h}_{m,n,k}^{ul}|^2P_{m,n,k}^{ul}+\sigma^2} \tag{26}$$

represent the MMSE for the DL and UL of UN$_k$ (see Appendix A). Problem $P(2)$ can be split into the time and weight resource (TRS) allocation problem and the power resource (PRS) allocation problem as shown in Appendix A. This is expressed as

$$\begin{aligned} \underset{\alpha,\{\psi_k\},\{\tau_k\},\omega_k^{dl},\omega_k^{ul}}{\text{minimize}} \quad & T_{RS} \\ \text{subject to} \quad & \alpha\sum_{k=1}^{K}\tau_k+(1-\alpha)\sum_{k=1}^{K}\psi_k=T,\ \omega_k^{ul}\ge 0 \\ & \sum_{n=1}^{N}\sum_{m=1}^{M}P_{m,n,k}^{ul}\le P_k^{ul}-P_c,\ \omega_k^{dl}\ge 0 \end{aligned} \tag{27}$$

and

$$\begin{aligned} \underset{\{P_{m,n,k}^{dl}\},\{P_{m,n,k}^{ul}\}}{\text{minimize}} \quad & P_{RS} \\ \text{subject to} \quad & \sum_{k=1}^{K}\sum_{n=1}^{N}\sum_{m=1}^{M}P_{m,n,k}^{dl}\le P_{0,max}^{dl} \\ & \sum_{n=1}^{N}\sum_{m=1}^{M}P_{m,n,k}^{ul}\le P_k^{ul}-P_c, \end{aligned} \tag{28}$$

respectively. Here, T_{RS} and P_{RS} are defined as

$$T_{RS}=\frac{MN}{2}\sum_{k=1}^{K}[x_k-\log_2(x_k)]+MN\sum_{k=1}^{K}[z_k-\log_2(z_k)] \tag{29}$$

and

$$\begin{aligned} P_{RS}=&\sum_{k=1}^{K}\sum_{n=1}^{N}\sum_{m=1}^{M}\log_2\Big(\frac{\sigma_k^2}{|\hat{h}_{m,n,k}^{dl}|^2P_{m,n,k}^{dl}+\sigma_k^2}\Big) \\ &+\sum_{k=1}^{K}\sum_{n=1}^{N}\sum_{m=1}^{M}\log_2\Big(\frac{\sigma^2}{|\hat{h}_{m,n,k}^{ul}|^2P_{m,n,k}^{ul}+\sigma^2}\Big). \end{aligned} \tag{30}$$

where $x_k=\frac{\alpha\tau_k\omega_k^{dl}T}{\log(2)}$ and $z_k=\frac{(1-\alpha)\psi_k\omega_k^{ul}T}{\log(2)}$.

III. Interference Cancellation and Optimization Solutions

In this section, the IIC algorithm and the detailed solution for WMMSE problem, $P(2)$, are presented. The optimized parameters obtained from solving $P(2)$ are used in a joint resource allocation algorithm to solve $P(1)$.

A. Iterative Interference Cancellation

In this subsection, we present the IIC algorithm used in this paper. As mentioned above, FBMC systems achieve improved frequency confinement compared to OFDM. However, this comes with the loss of complex orthogonality between subcarriers, resulting in high intrinsic interference. To remove the interference terms in (8) and (19), an IIC receiver is proposed in this paper. Notice from (8) and (19) that the interference terms are determined by the type of prototype filter, FFT/IFFT, and the fading channel effect. Unless a different prototype filter is selected, the interference terms vary mainly with the fading channel. After the initial decoding iteration, the receiver node (UN or BS), estimates the multipath channel responses ($\mathbf{H}_k^{dl}$ and $\mathbf{H}_k^{ul}$) and compute the effective channel matrices $\hat{\mathbf{H}}_k^{dl}$ and $\hat{\mathbf{H}}_k^{ul}$ using the filter response matrix $\mathbf{G}_{n,k}$ and the IFFT matrix $\mathbf{\Phi}$. In each iteration, the detected signal is remodulated to obtain estimates of the transmitted data symbols ($\mathbf{a}_{n,k}^{dl}$ or $\mathbf{a}_{n,k}^{ul}$). To obtain the ICI term in (19) the current estimated data symbol is multiplied by the estimated channel and filter responses. On the other hand, the ISI terms in (8) and (19) are obtained by multiplying the previous estimated data symbols by the estimated channel and filter responses. The calculated ICI and ISI terms are then subtracted from the received signal in order to achieve a better version of the demodulated signal in the next iteration. Detailed discussion on the IIC algorithm can be found in [3] and [25], and are shown in Algorithm 1.

Algorithm 1 IIC Algorithm

Set the maximum number of IIC iterations, I_{max}
Initialize iteration counter $i = 0$
while $i \leq I_{max}$ **do**
  if DL Communication **then**
    Estimate I_{ISI}^{dl} as described in Section III-A
    Subtract the estimated term from (8), i.e.
    $\hat{r}_{n,k}^{dl}(i+1) = \hat{r}_{n,k}^{dl}(i) - \hat{I}_{ISI}^{e,dl}$, let $i = i+1$
  else
    Estimate I_{ICI}^{ul} and I_{ISI}^{ul} as described in Section III-A
    Subtract the estimated terms from (19), i.e.
    $\hat{r}_{n,k}^{ul}(i+1) = \hat{r}_{n,k}^{ul}(i) - \hat{I}_{ICI}^{ul} - \hat{I}_{ISI}^{ul}$
  end if
  $i = i+1$
end while
Terminate

Algorithm 2 Power Resource Allocation Algorithm

Set time and weight allocations α, τ_k, ψ_k, ω_k^{dl} and ω_k^{ul}
repeat
  Calculate λ_k^{ul} using (33)
  Calculate $P_{m,n,k}^{ul}$ using (32)
  Find λ^{dl} using bisection method
  Calculate $P_{m,n,k}^{dl}$ using (31)
until (28) converges

Algorithm 3 WSR: Joint Resource Allocation Algorithm

Run line search to find $x^\star$ for the TRS optimization
Set time resource allocation to equal allocation
Calculate the weight using $\omega_k^\star = \frac{2x^\star K \log(2)}{T^2}$
Perform UL and DL IIC using Algorithm 1
Find $P_{m,n,k}^{dl}$ and $P_{m,n,k}^{ul}$, using Algorithm 2
Calculate sum-rate using the objective function in (23)

B. Optimal Resource Allocation (ORA)

The scheme for solving problem $P(1)$ is presented in this subsection. As shown in the previous section, $P(1)$ can be converted to a WMMSE problem, $P(2)$, which is further split into the TRS and PRS allocation problems. The solutions for the TRS and PRS problems are presented as follows:

1) TRS Optimization

The solution for the TRS allocation problem is presented in Theorem 1.

Theorem 1. *The optimal time and weight allocation for the WSR maximization problem is equal time and weights allocation, that is,* $\tau_1 = \ldots = \tau_K, \psi_1 = \ldots = \psi_K$ *and* $\omega_1^{dl} = \ldots = \omega_K^{dl}, \omega_1^{ul} = \ldots = \omega_K^{ul}$. *Hence,* $\alpha = 1/2$, $\tau_k = 1/K$, $\psi_k = 1/K$ *and* $\omega_k^{dl} = \omega_k^{ul} = \frac{2Kx^\star \log(2)}{T^2}$, *where* $x^\star$ *is the minimum value of the function* $f(x)$: *min*$[x - \log_2(x)]$.

Proof. See Appendix C □

2) PRS Optimization

The closed-form solutions for $P_{m,n,k}^{dl}$ and $P_{m,n,k}^{ul}$ are derived by differentiating the Lagrangian of (28) with respect to $P_{m,n,k}^{dl}$ and $P_{m,n,k}^{ul}$, respectively, and equating the differential to zero. Thus, the optimal DL and UL power allocation for UN_k can be express as

$$P_{m,n,k}^{dl\star} = \Big[\frac{1}{\log(2)A} - \frac{\sigma_k^2}{|\hat{h}_{m,n,k}^{dl}|^2}\Big] \tag{31}$$

and

$$P_{m,n,k}^{ul\star} = \Big[\frac{1}{\lambda_k^{ul\star}\log(2)} - \frac{\sigma^2}{|\hat{h}_{m,n,k}^{ul}|^2}\Big], \tag{32}$$

with $A = (\lambda^{dl\star} - \tau_k \sum_{n=1}^{N}\sum_{m=1}^{M}|\hat{h}_{m,n,k}^{dl}|^2 \sum_{j=1}^{K} \frac{\alpha\beta_j\lambda_j^{ul}}{(1-\alpha)\psi_j})$. Note that $\lambda^{dl\star}$ can be found using the bisection method and $\lambda_k^{ul\star}$ is given as

$$\lambda_k^{ul\star} = \frac{MN}{\log(2)\Big(B - P_c + \sum_{m=1}^{M}\frac{N\sigma_{z^{ul}}^2}{|\hat{h}_{m,n,k}^{ul}|^2}\Big)}, \tag{33}$$

with $B = \frac{\alpha\beta_k}{(1-\alpha)\psi_k}\sum_{j=1}^{K}\tau_j\sum_{n=1}^{N}\sum_{m=1}^{M}|\hat{h}_{m,n,j}^{dl}|^2 P_{m,n,j}^{dl}$.

Proof. See Appendix D □

As shown in Appendix D, the PRS problem is non-convex considering all variables jointly. Hence, an iterative algorithm is used to find the local optimum solutions of the DL and UL power allocations as shown in Algorithm 2.

3) WSR: Joint Resource Allocation

The optimal solutions of the TRS and PRS allocation problems in addition to the IIC algorithm are used in a joint resource allocation algorithm to find the maximum WSR as described in Algorithm 3. The performance of the optimal joint resource allocation algorithm is compared with five suboptimal schemes in the next section.

IV. Simulation Results

In this section, numerical results are presented for the proposed multi-user FBMC-based SWIPT system. A set up with 1.4MHz channel bandwidth and 4-QAM modulation is considered in the simulation. The noise spectral density is set as $N_0 = -174$ dBm/Hz. The UNs are assumed to be randomly distributed within a 10m radius around the BS. For the channel model, the Friis model is assumed for the path loss with $\kappa = 2$, $A = 1$ and $\tilde{d} = \lambda/4\pi$ [29]. Here, the energy conversion efficiency in the linear region of the EH receiver is set to 0.5 [32]. Unless otherwise stated, each plot assumes $K = 4$ UNs.

The optimal scheme is compared to five suboptimal schemes. The list of schemes presented in this section are OOOA, FEFA, FEOA, FOOA, EEOA and EEFA. The labelling of the various schemes use 'O' to represent optimal allocation, 'F' to represent fixed allocation, and 'E' to represent equal allocation. Also, each of the first three letters in the scheme names represent the type of allocation for a particular resource. The first letter represents the time allocation type, the second letter represents the power allocation type, the third letter represents the weight allocation type, and the last letter stands for 'allocation', that is, 'time', 'power', 'weight', 'allocation'. For example, OOOA means optimal time, optimal power, and optimal weights allocations. The various schemes' names and descriptions are described in Table I. Note that the fixed weight

TABLE I: List of Resources and Weights Allocation Schemes

Scheme	Considerations
OOOA	Optimal time, Optimal power and Optimal weights Allocations
FEFA	Fixed time, Equal power and Fixed weights Allocations
FEOA	Fixed time, Equal power and Optimal weights Allocations
FOOA	Fixed time, Optimal power and Optimal weights Allocations
EEOA	Equal time, Equal power and Optimal weights Allocations
EEFA	Equal time, Equal power and Fixed weights allocations

for each UN is set as 5 in the simulation. In addition, the fixed time allocation is achieved by randomly choosing the time allocated for each UN.

A. Proof and Convergence Simulations

In this subsection, simulation results on Theorem 1, and the convergence of Algorithm 2 are discussed.

1) TRS Allocation Results

For the time resource allocation, simulation results are presented to affirm Theorem 1. Fig. 2 shows plots for the T_{RS} of two UNs for DL (top half) and UL (bottom half) communications. It can be observed from these plots that the T_{RS} allocations of both UNs are similar for both UL and DL. This is consistent with Theorem 1, which states that the x value in (29) is the same for all UNs in both UL and DL. Also, time and weight allocations are the same. A similar deduction on the x value can be inferred from Fig. 3.

From Fig. 3 it is shown that both the x and z functions in (29) for DL and UL communications are the same and possess the same optimal value. This implies that, the BS only has to determine x once, and this can be done by using a simple line search method. In this paper, the Golden Section Search method is used [33]. Fig. 4 shows the convergence curve for the Golden Section Search method. From Fig. 4, it can be observed that the line search method converges after 10 iterations. This implies that determining the value of x and the time and weight allocations would not be computationally intensive.

2) PRS Allocation Results

Fig. 5 contains the convergence plot for the DL and UL power resource allocation algorithm. From the figure, it can be observed that 10 iterations is enough to achieve convergence in Algorithm 2. Hence, Algorithm 2 will also not result in a huge computational burden at the BS.

B. Harvested Power Simulations

In this subsection, simulation results on the energy harvested in the proposed system considering a non-linear EH model are presented. With the antenna threshold effect, the maximum amount of energy harvested by each UN can not exceed $\Delta_k P_{th}$, due to the non-linear behaviour of the EH receiver circuit. The saturation threshold power is set as 7 dBm [31].

Fig. 6 shows a plot of the amount of power harvested against the BS transmit power. From the figure, it can be observed that as the transmit power increases, the amount of power harvested by each UN increases. There is a constant increase until the EH threshold is reached, which occurs around $P^{dl}_{0,max} = 35$ dBm in Fig. 6. At this point, the power harvested cannot exceed

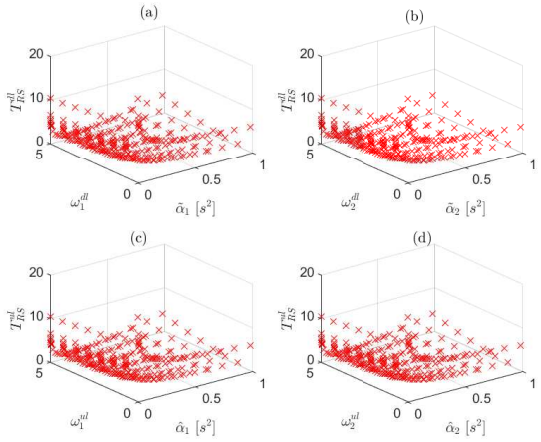

Fig. 2: $T^{(dl/ul)}_{RS}$ convexity plot with respect to the weight and time resource of two UNs, where $K = 2$. The 3D plot of T^{dl}_{RS} against the; (a) UN_1's DL weight and time allocation, (b) UN_2's DL weight and time allocation. The 3D plot of T^{ul}_{RS} against (c) UN_1's UL weight and time allocation, and (c) UN_2's UL weight and time allocation.

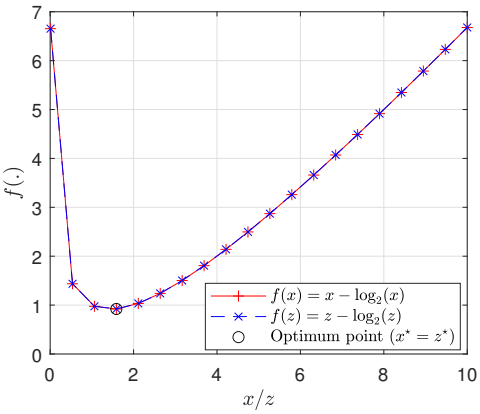

Fig. 3: Concavity plot of x-log and z-log functions

the threshold due to the non-linear behaviour of the energy harvester. It can be seen from Fig. 6 that, in the range of BS transmit power considered in the simulation, the EH receiver operates predominantly in the linear region for $P_{th} = 7$ dBm. If a different value of P_{th} is selected, the linear and non-linear regions of the EH receiver will be shifted accordingly. In addition, Fig. 6 shows that all the schemes with equal power allocation (i.e., FEFA, FEOA, EEOA, and EEFA) show a completely linear behaviour over the range BS transmit powers.

From Fig. 6 (a) it is shown that the available power at each UN is the same for the OOOA scheme because of the equal time allocation for the DL and UL communication. A similar behaviour is observed for the EEOA and the EEFA schemes. Also, in the FEFA scheme, UNs have equal power because of the equal power allocation in the DL. However, for the FOOA and FEOA schemes, since there are different time allocations for the DL and UL, the power harvested by each

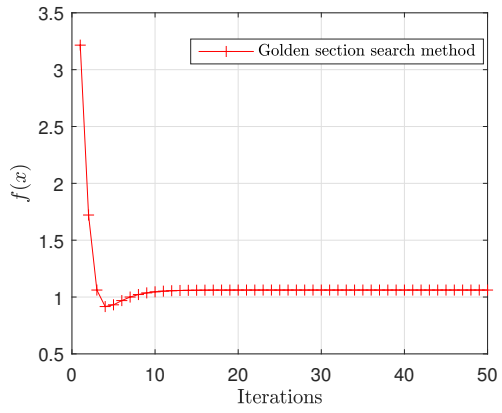

Fig. 4: Convergence plot for the x-log function

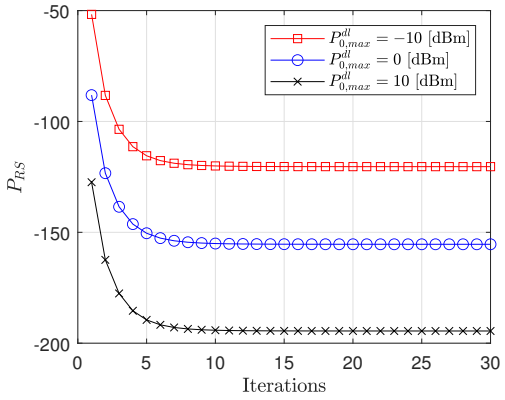

Fig. 5: P_{RS} function convergence plot with increasing number of algorithm iterations, where $K = 4$ and $P^{dl}_{0,max} = -10$dB, 0dB, and 10dB.

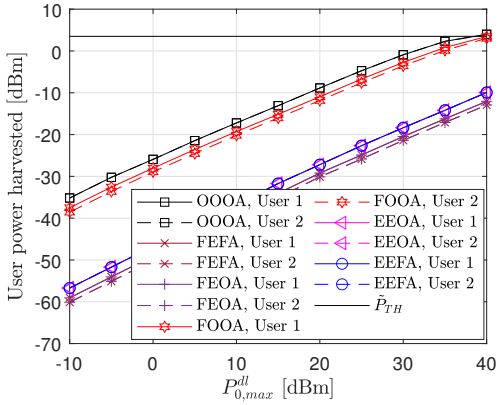

(a) User power harvested, $K = 2$.

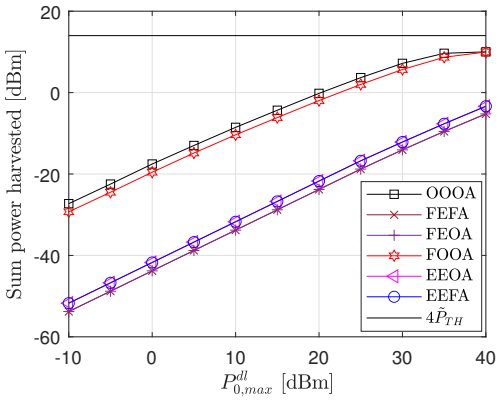

(b) Total power harvested, where $K = 4$

Fig. 6: Power harvested versus BS transmit power

UN is different. Fig. 6 (a) shows that for a BS transmit power of 30 dBm, each UN can harvest power of 0 dBm (1 mW) using the proposed optimal scheme. Assuming a typical IoT device that transmits data for a time duration of 450 ms with a maximum peak power of 200 mW and a duty cycle of 10%, it is shown in [34] that if the data transmission occurs every minute the average power transmitted over the period is 0.15 mW. This implies that the amount of energy harvested by the proposed scheme is more than six times the average transmit power required in the UL transmission of such an IoT device.

Unlike Fig. 6 (a), which shows the amount of power harvested by each UN, Fig. 6 (b) shows a plot of the total power harvested by 4 UNs. It can be observed from Fig. 6 (b) that the OOOA harvests the most energy and therefore has the highest power available for its UL communication. The order of decreasing amount of power harvested is as follows: OOOA, FOOA, FEFA, EEOA, EEFA, and FEFA. Fig. 7 shows the total amount of power harvested for each scheme with an increasing number of UNs. From the figure, it can be observed that the amount of energy harvested increases with an increasing number of UNs. For the schemes with equal power allocation, increasing the number of UNs beyond $K = 6$ does not significantly improve the amount of power harvested. This implies that optimizing the power allocated to each UN is necessary to maximize the amount of harvested energy.

C. Weighted Sum-Rate and Bit-Error-Probability Simulations

1) Weighted Sum-Rate

Fig. 8 (a) shows a plot of the weighted sum-rate against BS transmit power. From the plot the descending order of performance is as follows: OOOA, FOOA, EEOA, FEOA, EEFA and FEFA. It can be observed from the figure that the schemes with optimized resource allocations performed better compared to the schemes with fixed resource allocations. Also, it can be seen that the optimal scheme (OOOA) attains the best performance as expected. Note, however, that the scheme with fixed time allocation is only slightly poorer than the fully optimal scheme. This affirms the deductions made in the previous section that the fixed time allocation coincides with the optimal time allocation.

A plot showing the effect of increasing number of UNs on the weighted sum-rate is presented in Fig. 8 (b). As expected, with an increasing number of UNs the weighted sum-rate increases for all schemes except FEFA and EEFA. The weighted sum-rate for the FEFA and EEFA schemes remains constant as the number of UNs increases. This is due to the

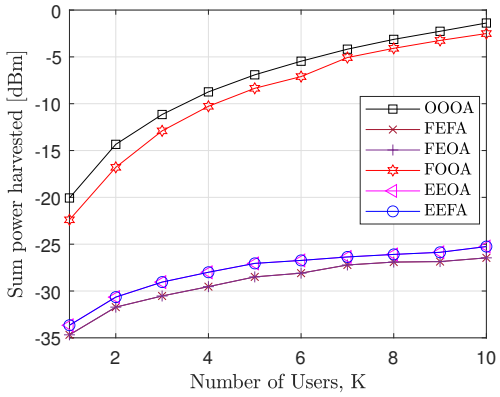

Fig. 7: Total power harvested versus increasing number of UNs, where $P_{0.max}^{dl} = 0$ dBm.

equal/fixed time, power and weight allocations. However, the schemes with either time, power or weight allocations being optimized compensates for the poor performance of the other equally allocated resources, as shown for the EEOA and FEOA curves.

2) Bit-Error-Probability

The bit-error-probability (BEP) expression for the k-th UN can be obtained as in [35], and is given by

$$BEP_k^i = \frac{1}{NM} \sum_{m=1}^{M} \sum_{n=1}^{N} Q(\sqrt{SNR_{m,n,k}^i}) \qquad (34)$$

where $Q(\cdot)$ denotes the Q-function and i is the transmission phase, i.e. DL or UL.

Figs. 9 (a) and 9 (b) show the average BEP for the DL and the UL communications, respectively. From Fig. 9 (a), all schemes with equal power allocations have the same BEP values. In addition, the OOOA has a similar BEP when compared to the FOOA scheme due to the use of the DL optimal power and weight allocations for both schemes. Fig. 9 (b) considers the UL BEP for the various schemes. The UL depends on the UL power for each UN, which in turn depends on the amount of power harvested during the DL communication phase (i.e., the power available depends on both the DL and UL time allocations). As expected, OOOA and FOOA have better performance compared to the other schemes. In addition, the UL BEP of EEFA, EEOA, FEFA and FEOA schemes are different due to both the time (i.e., equal DL and UL time allocations) and the optimal UL power allocation in each scheme. As can be seen from 9 (b), a BEP of 10^{-4} can be achieved by the OOOA scheme on the uplink when the BS transmits with a power of 10 dBm.

D. Implementation and Complexity Analysis

Here, the complexity analysis for each proposed SWIPT protocol (i.e., OOOA, FEFA, FEOA, FOOA, EEOA and EEFA) is presented. A centralized processing approach is utilized for the optimal resource allocation, in which all the processing involved in solving problem $P(1)$ are implemented at the BS. This is because the BS has a larger processing

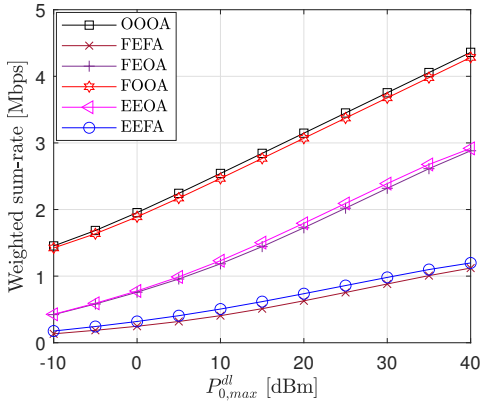

(a) $K = 4$

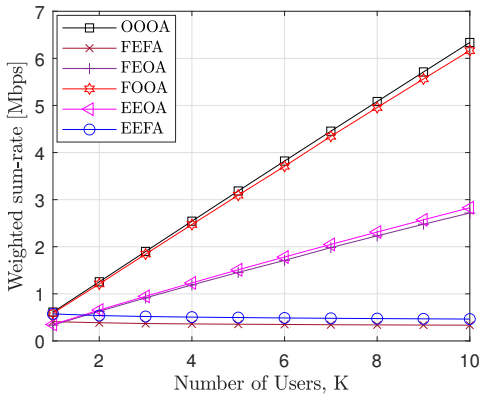

(b) $P_{0,max}^{dl} = 10$ dBm

Fig. 8: Weighted sum-rate versus (a) BS transmit power (b) number of UNs

capacity, can obtain the global CSI and has a constant power supply. The optimal time and power allocations and weight values are sent to the UNs in the DL phase.

Now, considering the computational complexity, assume that the processing complexity of the optimal joint resource allocation algorithm, IIC algorithm, power allocation algorithm and the line search method are given by $\mathcal{O}(I_{WSR})$, $\mathcal{O}(I_{IIC})$, $\mathcal{O}(I_{PWR})$, and $\mathcal{O}(I_{LSM})$, respectively. In addition, the computation of an arithmetic operation is defined as $\mathcal{O}(A)$. Note that the big O value for each algorithm includes all the arithmetic calculations involved in that algorithm. For example $\mathcal{O}(I_{WSR})$ consists of the computational complexities of the IIC algorithm, power allocation algorithm and the line search algorithm for finding the time and weight allocations. Hence the order of complexity in this simulation follows as $\mathcal{O}(I_{WSR}) \gg \mathcal{O}(I_{IIC}) \geq \mathcal{O}(I_{PWR}) > \mathcal{O}(I_{LSM}) \gg \mathcal{O}(A)$. The value of $\mathcal{O}(I_{IIC})$ may be greater or equal to $\mathcal{O}(I_{PWR})$ because the IIC algorithm depends on the complexity of the FBMC modulation and demodulation and the number of iteration [3]. From the simulation results, the line search method converges quickly and involves fewer computations compared to the power algorithm. Also, a lower number of computations is needed to perform an arithmetic operation.

First, the OOOA scheme runs the joint resource allocation

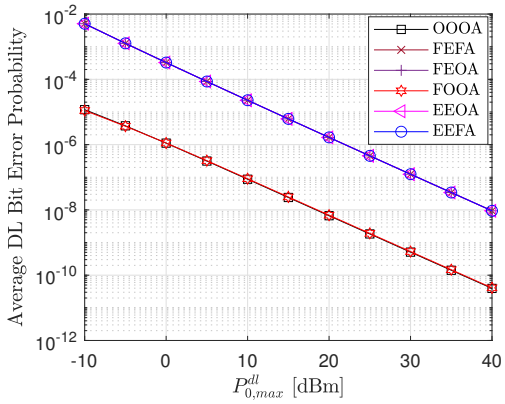

(a) DL

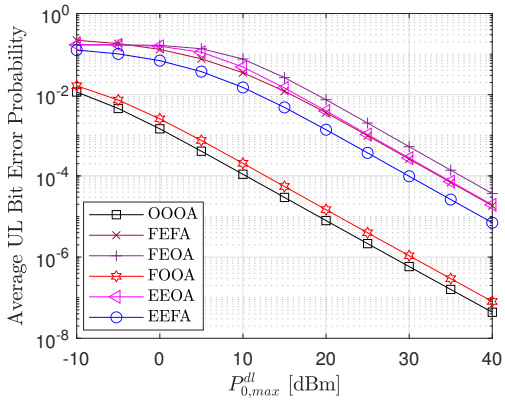

(b) UL

Fig. 9: Average BEP versus source transmit power, where $K = 4$

algorithm with complexity $\mathcal{O}(I_{WSR})$. Hence, the complexity of the OOOA scheme is given as $\mathcal{O}(I_{WSR}) = \mathcal{O}(I_{IIC}) + \mathcal{O}(I_{PWR}) + \mathcal{O}(I_{LSM}) + \mathcal{O}(A)$. Next, in the FEFA and EEFA schemes only the IIC algorithm is implemented. Thus, their complexity is given by $\mathcal{O}(I_{IIC})$. The FEOA and EEOA schemes perform the IIC algorithm and some arithmetic operations to obtain the optimal weights. Therefore, the complexity in both schemes is given as $\mathcal{O}(I_{IIC}) + \mathcal{O}(A)$. Finally, for the FOOA scheme the IIC algorithm, power allocation algorithm and arithmetic operations are implemented, with complexity given as $\mathcal{O}(I_{IIC}) + \mathcal{O}(I_{PWR}) + \mathcal{O}(A)$. The complexity analysis for the centralized approach is presented in Table II.

Note that the centralized approach reduces the processing complexity and power consumption at the UN. However, each UN must perform IIC at the information receiver, which requires local CSI. A detailed complexity analysis of the IIC algorithm is given in [3], including a discussion on alternative approaches to reducing this complexity. It is shown in [3] that only a few IIC iterations are sufficient to remove the intrinsic interference in FBMC. Furthermore, the batteries at the UNs are recharged continuously, while the IIC processing is only needed when the node receives a downlink packet. In most IoT applications, e.g. wireless sensor networks, the amount of downlink data received is very small compared to the uplink transmission. As such the IIC processing will be implemented periodically and can therefore be supported by the harvested power in the batteries. A full analysis of the power consumption of the signal processing at the UNs is beyond the scope of this paper.

TABLE II: Complexity Different Schemes

Scheme	Node	Computational Complexity
OOOA	BS	$\mathcal{O}(I_{IIC}) + \mathcal{O}(I_{PWR}) + \mathcal{O}(I_{LSM}) + \mathcal{O}(A)$
	UN	$\mathcal{O}(I_{IIC})$
FEFA	BS	$\mathcal{O}(I_{IIC})$
	UN	$\mathcal{O}(I_{IIC})$
FEOA	BS	$\mathcal{O}(I_{IIC}) + \mathcal{O}(A)$
	UN	$\mathcal{O}(I_{IIC})$
FOOA	BS	$\mathcal{O}(I_{IIC}) + \mathcal{O}(I_{PWR}) + \mathcal{O}(A)$
	UN	$\mathcal{O}(I_{IIC})$
EEOA	BS	$\mathcal{O}(I_{IIC}) + \mathcal{O}(A)$
	UN	$\mathcal{O}(I_{IIC})$
EEFA	BS	$\mathcal{O}(I_{IIC})$
	UN	$\mathcal{O}(I_{IIC})$

V. Conclusion

In a multi-user IoT network with energy-constrained devices, SWIPT can serve as a source of power for UNs and provide network self-sustainability. In addition, FBMC is a promising waveform for future IoT applications due to its high spectral efficiency and suitability for asynchronous transmissions. This paper investigated the combination of SWIPT with FBMC systems for IoT networks. Specifically, a multi-user FBMC-based SWIPT system is considered where each UN has two antennas, one for EH and the other for ID. A practical non-linear model is considered at the energy receiver, whereas an IIC receiver is employed at the information receiver. A WMMSE problem is solved to optimize the time, weight and power allocations. Five sub-optimal schemes are proposed for comparison. The complexity analysis of the proposed optimal and sub-optimal schemes is also presented. The results show that the optimal time and weight allocations coincide with equal time and weight allocation. In terms of average sum-rate at BS transmit power of 20 dBm, the optimal scheme outperforms the scheme with equal time, equal power, and optimal weight allocation by about 40%. In summary, the proposed FBMC-based SWIPT system is a promising technique for future IoT applications due to the capability of achieving network self-sustainability, high spectral efficiency and suitability for asynchronous transmissions simultaneously. Future work will investigate a model in which FBMC-based SWIPT IoT devices coexist with OFDM-based cellular devices.

Appendix A
WSR and WMMSE Relationship

From equations (8) and (19), the DL and UL mean squared error (MSE) for each UN is given as

$$\begin{aligned} e^{dl}_{m,n,k} &= |\hat{h}^{dl}_{m,n,k} P^{dl}_{m,n,k} v^{dl}_{m,n,k} - 1|^2 + \sigma^2_k |v^{dl}_{m,n,k}|^2 \\ &= 1 + |\hat{h}^{dl}_{m,n,k}|^2 |v^{dl}_{m,n,k}|^2 P^{dl}_{m,n,k} \\ &\quad + 2\hat{h}^{dl}_{m,n,k} v^{dl}_{m,n,k} \sqrt{P^{dl}_{m,n,k}} + \sigma^2_k |v^{dl}_{m,n,k}|^2 \end{aligned} \tag{35}$$

and

$$\begin{aligned} e^{ul}_{m,n,k} &= |\hat{h}^{ul}_{m,n,k} P^{ul}_{m,n,k} v^{ul}_{m,n,k} - 1|^2 + \sigma^2 |v^{ul}_{m,n,k}|^2 \\ &= 1 + |\hat{h}^{ul}_{m,n,k}|^2 |v^{ul}_{m,n,k}|^2 P^{ul}_{m,n,k} \\ &\quad + 2\hat{h}^{ul}_{m,n,k} v^{ul}_{m,n,k} \sqrt{P^{ul}_{m,n,k}} + \sigma^2 |v^{ul}_{m,n,k}|^2, \end{aligned} \tag{36}$$

where $v^{dl}_{m,n,k}$ and $v^{ul}_{m,n,k}$ are the MSE receiver filters for the DL and UL, respectively. To acquire the minimum MSE (MMSE) for the DL and UL, the optimal $v^{dl}_{m,n,k}$ and $v^{ul}_{m,n,k}$ are deduced from $\frac{\partial e^{dl}_{m,n,k}}{\partial v^{dl}_{m,n,k}} = 0$ and $\frac{\partial e^{ul}_{m,n,k}}{\partial v^{ul}_{m,n,k}} = 0$ respectively as

$$\begin{aligned} v^{dl\star}_{m,n,k} &= \frac{\hat{h}^{dl}_{m,n,k} \sqrt{P^{dl}_{m,n,k}}}{|\hat{h}^{dl}_{m,n,k}|^2 P^{dl}_{m,n,k} + \sigma^2_k}, \quad \text{and} \\ v^{ul\star}_{m,n,k} &= \frac{h^{ul}_{m,k} \sqrt{P^{ul}_{m,n,k}}}{|\hat{h}^{ul}_{m,n,k}|^2 P^{ul}_{m,n,k} + \sigma^2}. \end{aligned} \tag{37}$$

Substituting $v^{dl\star}_{m,n,k}$ and $v^{ul\star}_{m,n,k}$ into (35) and (36), the MMSE for the DL and UL are derived as

$$\begin{aligned} e^{dl}_{m,n,k} &= \frac{\sigma^2_k}{|\hat{h}^{dl}_{m,n,k}|^2 P^{dl}_{m,n,k} + \sigma^2_k}, \quad \text{and} \\ e^{ul}_{m,n,k} &= \frac{\sigma^2}{|\hat{h}^{ul}_{m,n,k}|^2 P^{ul}_{m,n,k} + \sigma^2}, \end{aligned} \tag{38}$$

respectively. Using (38), the weighted MMSE (WMMSE) problem is expressed as

$$\begin{aligned} \underset{L_g}{\text{minimize}} \quad & \sum_{k=1}^{K} \sum_{m=1}^{M} \sum_{n=1}^{N} \left[\bar{\omega}^{dl}_k e^{dl}_{m,n,k} + \bar{\omega}^{ul}_k e^{ul}_{m,n,k} \right] \\ \text{subject to} \quad & \sum_{m=1}^{M} \sum_{n=1}^{N} P^{dl}_{m,n,k} \le P^{dl}_{0,max},\ \bar{\omega}^{ul}_k \ge 0 \\ & \sum_{k=1}^{K} \sum_{m=1}^{M} \sum_{n=1}^{N} P^{ul}_{m,n,k} \le P^{ul}_k - P_c,\ \bar{\omega}^{dl}_k \ge 0, \\ & \alpha \sum_{k=1}^{K} \tau_k + (1-\alpha) \sum_{k=1}^{K} \psi_k = T, \end{aligned} \tag{39}$$

where $L_g = [\alpha, \{P^{dl}_{m,n,k}\}, \{P^{ul}_{m,n,k}\}, \{\psi_k\}, \{\tau_k\}, \{\bar{\omega}^{dl}_k\}, \{\bar{\omega}^{ul}_k\}]$. Also, $\bar{\omega}^{dl}_k$ and $\bar{\omega}^{ul}_k$ are the WMMSE weights for the DL and UL, respectively. The WSR problem based on the MMSE is defined as

$$\begin{aligned} \underset{L_g}{\text{maximize}} \quad & \sum_{k=1}^{K} \sum_{m=1}^{M} \sum_{n=1}^{N} \left[\omega^{dl}_k \bar{R}^{dl}_{m,n,k} + \omega^{ul}_k \bar{R}^{ul}_{m,n,k} \right] \\ \text{subject to} \quad & \sum_{m=1}^{M} \sum_{n=1}^{N} P^{dl}_{m,n,k} \le P^{dl}_{0,max},\ \omega^{ul}_k \ge 0, \\ & \sum_{k=1}^{K} \sum_{m=1}^{M} \sum_{n=1}^{N} P^{ul}_{m,n,k} \le P^{ul}_k - P_c,\ \omega^{dl}_k \ge 0, \\ & \alpha \sum_{k=1}^{K} \tau_k + (1-\alpha) \sum_{k=1}^{K} \psi_k = T, \end{aligned} \tag{40}$$

where $L_g = [\alpha, \{P^{dl}_{m,n,k}\}, \{P^{ul}_{m,n,k}\}, \{\psi_k\}, \{\tau_k\}, \{\omega^{dl}_k\}, \{\omega^{ul}_k\}]$ and $\bar{R}^{dl}_{m,n,k} = -log_2(e^{dl}_{m,n,k})$ and $\bar{R}^{ul}_{m,n,k} = -log_2(e^{ul}_{m,n,k})$.

The next step is to establish the relationship between the WSR and WMMSE. The Lagrangian and KKT condition of the WMMSE problem with respect to $P^{dl}_{m,n,k}$ and $P^{ul}_{m,n,k}$ are deduced as

$$\begin{aligned} L_{\{WMMSE\}} &= \sum_{k=1}^{K} \bar{\omega}^{dl}_k \sum_{m=1}^{M} \sum_{n=1}^{N} e^{dl}_{m,n,k} - \sum_{k=1}^{K} \sum_{m=1}^{M} \sum_{n=1}^{N} \log_2(\bar{\omega}^{dl}_k) \\ &\quad + \sum_{k=1}^{K} \bar{\omega}^{ul}_k \sum_{m=1}^{M} \sum_{n=1}^{N} e^{ul}_{m,n,k} - \sum_{k=1}^{K} \sum_{m=1}^{M} \sum_{n=1}^{N} \log_2(\bar{\omega}^{ul}_k) + \mu T \\ &\quad - \lambda^{dl} \Big(\sum_{k=1}^{K} \sum_{m=1}^{M} \sum_{n=1}^{N} P^{dl}_{m,n,k} - P^{dl}_{0,max} \Big) - \mu(1-\alpha) \sum_{k=1}^{K} \psi_k \\ &\quad - \sum_{k=1}^{K} \lambda^{ul}_k \Big(\sum_{m=1}^{M} \sum_{n=1}^{N} P^{ul}_{m,n,k} + P_c - P^{dl}_k \Big) - \mu\alpha \sum_{k=1}^{K} \tau_k, \end{aligned} \tag{41}$$

$$\begin{aligned} \frac{\partial L_{\{WMMSE\}}}{\partial P^{dl}_{m,n,k}} &= -\bar{\omega}^{dl}_k \frac{\sigma^2_k |\hat{h}^{dl}_{m,n,k}|^2}{(|\hat{h}^{dl}_{m,n,k}|^2 P^{dl}_{m,n,k} + \sigma^2_k)^2} - \lambda^{dl} \\ &\quad + \tau_k |\hat{h}^{dl}_{m,n,k}|^2 \sum_{j=1}^{K} \frac{\lambda^{ul}_j \beta_j \alpha}{(1-\alpha)\psi_j}, \end{aligned} \tag{42}$$

and

$$\frac{\partial L_{\{WMMSE\}}}{\partial P^{ul}_{m,n,k}} = -\bar{\omega}^{dl}_k \frac{\sigma^2_k |\hat{h}^{dl}_{m,n,k}|^2}{(|\hat{h}^{dl}_{m,n,k}|^2 P^{dl}_{m,n,k} + \sigma^2_k)^2} - \lambda^{ul}. \tag{43}$$

Similarly, the Lagrangian and KKT conditions for the WSR problem with respect to $P^{dl}_{m,n,k}$ and $P^{ul}_{m,n,k}$ are deduced as

$$\begin{aligned} L_{\{WSR\}} &= -\sum_{k=1}^{K} \alpha\tau_k \omega^{dl}_k T \sum_{m=1}^{M} \sum_{n=1}^{N} \log_2 \Big(\frac{\sigma^2_{z^{dl}}}{|\hat{h}^{dl}_{m,n,k}|^2 P^{dl}_{m,n,k} + \sigma^2_{z^{dl}}} \Big) \\ &\quad - \sum_{k=1}^{K} (1-\alpha)\psi_k \omega^{ul}_k T \sum_{m=1}^{M} \sum_{n=1}^{N} \log_2 \Big(\frac{\sigma^2_{z^{ul}}}{|\hat{h}^{ul}_{m,n,k}|^2 P^{ul}_{m,n,k} + \sigma^2_{z^{ul}}} \Big) \\ &\quad - \lambda^{dl} \Big(\sum_{k=1}^{K} \sum_{m=1}^{M} \sum_{n=1}^{N} P^{dl}_{m,n,k} - P^{dl}_{0,max} \Big) - \mu(1-\alpha) \sum_{k=1}^{K} \psi_k \\ &\quad - \sum_{k=1}^{K} \lambda^{ul}_k \Big(\sum_{m=1}^{M} \sum_{n=1}^{N} P^{ul}_{m,n,k} + P_c - P^{dl}_k \Big) - \mu\alpha \sum_{k=1}^{K} \tau_k + \mu T, \end{aligned} \tag{44}$$

$$\begin{aligned} \frac{\partial L_{\{WSR\}}}{\partial P^{dl}_{m,n,k}} &= \frac{\alpha\tau_k \omega^{dl}_k T}{\log(2)} \Big(e^{dl}_{m,n,k} \Big)^{-1} \Big(\frac{\sigma^2_{z^{dl}} |\hat{h}^{dl}_{m,n,k}|^2}{(|\hat{h}^{dl}_{m,n,k}|^2 P^{dl}_{m,n,k} + \sigma^2_{z^{dl}})^2} \Big) \\ &\quad - \lambda^{dl} + \tau_k |\hat{h}^{dl}_{m,n,k}|^2 \sum_{j=1}^{K} \frac{\lambda^{ul}_j \beta_j \alpha}{(1-\alpha)\psi_j}, \end{aligned} \tag{45}$$

and

$$\begin{aligned} \frac{\partial L_{\{WSR\}}}{\partial P^{ul}_{m,n,k}} &= \frac{(1-\alpha)\psi_k \omega^{ul}_k T}{\log(2)} \Big(e^{ul}_{m,n,k} \Big)^{-1} \\ &\quad \times \Big(\frac{\sigma^2_{z^{ul}} |\hat{h}^{ul}_{m,n,k}|^2}{(|\hat{h}^{ul}_{m,n,k}|^2 P^{ul}_{m,n,k} + \sigma^2_{z^{ul}})^2} \Big) - \lambda^{ul}_k. \end{aligned} \tag{46}$$

Comparing (42) and (43) to (45) and (46), respectively, the WMMSE weights can be estimated as

$$\begin{aligned}\bar{\omega}_k^{dl} &= \frac{\alpha\tau_k\omega_k^{dl}T}{\log(2)}\Big(e_{m,n,k}^{dl}\Big)^{-1} \text{ and} \\ \bar{\omega}_k^{ul} &= \frac{(1-\alpha)\psi_k\omega_k^{ul}T}{\log(2)}\Big(e_{m,n,k}^{ul}\Big)^{-1}\end{aligned} \tag{47}$$

making the WSR and WMMSE problems equivalent. Now, inserting (47) into (41) results in

$$\begin{aligned}L_{\{WMMSE\}} = &\frac{MN}{2}\sum_{k=1}^{K}\Big[\frac{\alpha\tau_k\omega_k^{dl}T}{\log(2)} - \log_2\Big(\frac{\alpha\tau_k\omega_k^{dl}T}{\log(2)}\Big)\Big] \\ &+ \sum_{k=1}^{K}\sum_{m=1}^{M}\sum_{n=1}^{N}\log_2\Big(\frac{\sigma_{z^{dl}}^2}{|\hat{h}_{m,n,k}^{dl}|^2P_{m,n,k}^{dl}+\sigma_{z^{dl}}^2}\Big) \\ &+ MN\sum_{k=1}^{K}\Big[\frac{(1-\alpha)\psi_k\omega_k^{ul}T}{\log(2)} - \log_2\Big(\frac{(1-\alpha)\psi_k\omega_k^{ul}T}{\log(2)}\Big)\Big] \\ &+ \sum_{k=1}^{K}\sum_{m=1}^{M}\sum_{n=1}^{N}\log_2\Big(\frac{\sigma_{z^{ul}}^2}{|\hat{h}_{m,n,k}^{ul}|^2P_{m,n,k}^{ul}+\sigma_{z^{ul}}^2}\Big) \\ &- \lambda^{dl}\Big(\sum_{k=1}^{K}\sum_{m=1}^{M}\sum_{n=1}^{N}P_{m,n,k}^{dl} - P_{0,max}^{dl}\Big) \\ &- \sum_{k=1}^{K}\lambda_k^{ul}\Big(\sum_{m=1}^{M}\sum_{n=1}^{N}P_{m,n,k}^{ul} + P_c - P_k^{dl}\Big) \\ &- \mu\Big(\alpha\sum_{k=1}^{K}\tau_k + (1-\alpha)\sum_{k=1}^{K}\psi_k - T\Big),\end{aligned} \tag{48}$$

From (48), the WMMSE problem can be split into the time and weight resource allocation problem and the power resource allocation problem as

$$\begin{aligned}\underset{\alpha,\{\psi_k\},\{\tau_k\},\omega_k^{dl},\omega_k^{ul}}{\text{minimize}} \quad & T_{RS} \\ \text{subject to} \quad & \alpha\sum_{k=1}^{K}\tau_k + (1-\alpha)\sum_{k=1}^{K}\psi_k = T,\ \omega_k^{ul} \geq 0, \\ & \sum_{m=1}^{M}\sum_{n=1}^{N}P_{m,n,k}^{ul} \leq P_k^{ul} - P_c,\ \omega_k^{dl} \geq 0,\end{aligned} \tag{49}$$

and

$$\begin{aligned}\underset{\{P_{m,n,k}^{dl}\},\{P_{m,n,k}^{ul}\}}{\text{minimize}} \quad & P_{RS} \\ \text{subject to} \quad & \sum_{k=1}^{K}\sum_{m=1}^{M}\sum_{n=1}^{N}P_{m,n,k}^{dl} \leq P_{0,max}^{dl} \\ & \sum_{m=1}^{M}\sum_{n=1}^{N}P_{m,n,k}^{ul} \leq P_k^{ul} - P_c,\end{aligned} \tag{50}$$

where T_{RS} and P_{RS} are defined in (29) and (30), respectively. Therefore, the weights and time allocation can be determined from (49), while the power allocation can be determined from (50). ■

APPENDIX B
CONVEXITY PROOF OF TIME AND WEIGHT RESOURCE ALLOCATION PROBLEM

The time and weight resource problem can be split into two sub problems, the DL time and weight allocation problem and the UL time and weight allocation problem. The Lagrangian of the individual problems are defined respectively as

$$\begin{aligned}L_{RS}^{dl} = &\frac{MN}{2}\sum_{k=1}^{K}\Big[\frac{\alpha\tau_k\omega_k^{dl}T}{\log(2)} - \log_2\Big(\frac{\alpha\tau_k\omega_k^{dl}T}{\log(2)}\Big)\Big] \\ &- \mu\Big(\alpha\sum_{k=1}^{K}\tau_k + (1-\alpha)\sum_{k=1}^{K}\psi_k - T\Big) \\ &- \sum_{k=1}^{K}\lambda_k^{ul}\Big(\sum_{m=1}^{M}\sum_{n=1}^{N}P_{m,n,k}^{ul} + P_c \\ &- \frac{\alpha\beta_k}{(1-\alpha)\psi_k}\sum_{j=1}^{K}\tau_j\sum_{m=1}^{M}\sum_{n=1}^{N}|\hat{h}_{m,n,j}^{dl}|^2P_{m,n,j}^{dl}\Big).\end{aligned} \tag{51}$$

$$\begin{aligned}L_{RS}^{ul} = &MN\sum_{k=1}^{K}\Big[\frac{(1-\alpha)\psi_k\omega_k^{ul}T}{\log(2)} - \log_2\Big(\frac{(1-\alpha)\psi_k\omega_k^{ul}T}{\log(2)}\Big)\Big] \\ &- \mu\Big(\alpha\sum_{k=1}^{K}\tau_k + (1-\alpha)\sum_{k=1}^{K}\psi_k - T\Big) \\ &- \sum_{k=1}^{K}\lambda_k^{ul}\Big(\sum_{m=1}^{M}\sum_{n=1}^{N}P_{m,n,k}^{ul} + P_c \\ &- \frac{\alpha\beta_k}{(1-\alpha)\psi_k}\sum_{j=1}^{K}\tau_j\sum_{m=1}^{M}\sum_{n=1}^{N}|\hat{h}_{m,n,j}^{dl}|^2P_{m,n,j}^{dl}\Big).\end{aligned} \tag{52}$$

Concentrating on (51), the first derivatives of L_{RS}^{dl} with respect to the time and weight variables α, τ_k, and ω_k^{dl} are respectively given as

$$\begin{aligned}\frac{\partial L_{RS}^{dl}}{\partial\alpha} = &\frac{MN}{2}\sum_{k=1}^{K}\Big[\frac{\tau_k\omega_k^{dl}T}{\log(2)} - \frac{1}{\alpha\log(2)}\Big] - \mu\sum_{k=1}^{K}\tau_k \\ &+ \sum_{k=1}^{K}\frac{\lambda_k^{ul}\beta_k}{(1-\alpha)^2\psi_k}\sum_{j=1}^{K}\tau_j\sum_{m=1}^{M}\sum_{n=1}^{N}|\hat{h}_{m,n,j}^{dl}|^2P_{m,n,j}^{dl}.\end{aligned} \tag{53}$$

$$\begin{aligned}\frac{\partial L_{RS}^{dl}}{\partial\tau_k} = &\frac{MN}{2}\Big[\frac{\alpha\omega_k^{dl}T}{\log(2)} - \frac{1}{\tau_k\log(2)}\Big] - \alpha\mu \\ &+ \sum_{m=1}^{M}\sum_{n=1}^{N}|\hat{h}_{m,n,k}^{dl}|^2P_{m,n,k}^{dl}\sum_{j=1}^{K}\frac{\lambda_j^{ul}\beta_j\alpha}{(1-\alpha)\psi_j},\end{aligned} \tag{54}$$

and

$$\frac{\partial L_{RS}^{dl}}{\partial\omega_k^{dl}} = \frac{MN}{2}\Big[\frac{\alpha\tau_kT}{\log(2)} - \frac{1}{\omega_k^{dl}\log(2)}\Big], \tag{55}$$

The Second derivatives of L_{RS}^{dl} with respect to the time variables α, τ_k, and ω_k^{dl} are respectively derived as

$$\begin{aligned}\frac{\partial^2 L_{RS}^{dl}}{\partial\alpha^2} = &\frac{MNK}{2\log(2)\alpha^2} \\ &- \sum_{k=1}^{K}\frac{2\lambda_k^{ul}\beta_k}{(1-\alpha)^3\psi_k}\sum_{j=1}^{K}\tau_j\sum_{m=1}^{M}\sum_{n=1}^{N}|\hat{h}_{m,n,j}^{dl}|^2P_{m,n,j}^{dl}\end{aligned} \tag{56}$$

$$\frac{\partial^2 L_{RS}^{dl}}{\partial \tau_k^2} = \frac{MN}{\tau_k^2 2\log(2)} \tag{57}$$

$$\frac{\partial^2 L_{RS}^{dl}}{\partial \omega_k^{dl^2}} = \frac{MN}{\omega_k^{dl^2} 2\log(2)}. \tag{58}$$

$$\frac{\partial^2 L_{RS}^{dl}}{\partial \tau_k \partial \alpha} = \frac{MN\omega_k^{dl}T}{2\log(2)} - \mu + \sum_{m=1}^{M}\sum_{n=1}^{N}|\hat{h}_{m,n,k}^{dl}|^2 P_{m,n,k}^{dl} \sum_{j=1}^{K} \frac{\lambda_j^{ul}\beta_j}{(1-\alpha)^2\psi_j} \tag{59}$$

$$\frac{\partial^2 L_{RS}^{dl}}{\partial \omega_k^{dl} \partial \alpha} = \frac{MN\tau_k T}{2\log(2)} \tag{60}$$

The Hermitian matrix for the DL time and weight resource allocation problem Lagrangian is represented as

$$\begin{bmatrix} & \alpha & \tau_k & \omega_k^{dl} \\ \alpha & + & + & + \\ \tau_k & + & + & + \\ \omega_k^{dl} & + & + & + \end{bmatrix}. \tag{61}$$

From the Hermitian matrix all the second derivatives have positive values. Therefore, the DL time and weight allocation problem is convex with respect to all its variables.

Next, the convexity of the UL time and weight allocation problem is checked. The first derivatives of L_{RS}^{ul} with respect to the time and weight variables α, ψ_k, and ω_k^{ul} are respectively given as

$$\frac{\partial L_{RS}^{ul}}{\partial \alpha} = \mu\sum_{k=1}^{K}\psi_k - MN\sum_{k=1}^{K}\Big[\frac{\psi_k\omega_k^{ul}T}{\log(2)} - \frac{1}{(1-\alpha)\log(2)}\Big] + \sum_{k=1}^{K}\frac{\lambda_k^{ul}\beta_k}{(1-\alpha)^2\psi_k}\sum_{j=1}^{K}\tau_j\sum_{m=1}^{M}\sum_{n=1}^{N}|\hat{h}_{m,n,j}^{dl}|^2 P_{m,n,j}^{dl} \tag{62}$$

$$\frac{\partial L_{RS}^{ul}}{\partial \psi_k} = MN\Big[\frac{(1-\alpha)\omega_k^{ul}T}{\log(2)} - \frac{1}{\psi_k\log(2)}\Big] - (1-\alpha)\mu - \frac{\lambda_k^{ul}\beta_k\alpha}{(1-\alpha)\psi_k^2}\sum_{j=1}^{K}\tau_j\sum_{m=1}^{M}\sum_{n=1}^{N}|\hat{h}_{m,n,j}^{dl}|^2 P_{m,n,j}^{dl}, \tag{63}$$

$$\frac{\partial L_{RS}^{ul}}{\partial \omega_k^{ul}} = MN\Big[\frac{(1-\alpha)\psi_k T}{\log(2)} - \frac{1}{\omega_k^{ul}\log(2)}\Big]. \tag{64}$$

The Second derivatives of L_{RS}^{ul} with respect to the time variables α, ψ_k, and ω_k^{ul} are respectively derived as

$$\frac{\partial^2 L_{RS}^{ul}}{\partial \alpha^2} = \frac{MNK}{(1-\alpha)^2\log(2)} - \sum_{k=1}^{K}\frac{2\lambda_k^{ul}\beta_k}{(1-\alpha)^3\psi_k}\sum_{j=1}^{K}\tau_j\sum_{m=1}^{M}\sum_{n=1}^{N}|\hat{h}_{m,n,j}^{dl}|^2 P_{m,n,j}^{dl} \tag{65}$$

$$\frac{\partial^2 L_{RS}^{ul}}{\partial \psi_k^2} = \frac{MN}{\psi_k^2\log(2)} + \frac{2\lambda_k^{ul}\beta_k}{(1-\alpha)\psi_k^3}\sum_{j=1}^{K}\tau_j\sum_{m=1}^{M}\sum_{n=1}^{N}|\hat{h}_{m,n,j}^{dl}|^2 P_{m,n,j}^{dl} \tag{66}$$

$$\frac{\partial^2 L_{RS}^{ul}}{\partial \psi_k \partial \alpha} = -\frac{MN\omega_k^{ul}T}{\log(2)} + \mu - \frac{\lambda_k^{ul}\beta_k}{(1-\alpha)^2\psi_k^2}\sum_{j=1}^{K}\tau_j\sum_{m=1}^{M}\sum_{n=1}^{N}|\hat{h}_{m,n,j}^{dl}|^2 P_{m,n,j}^{dl} \tag{67}$$

$$\frac{\partial^2 L_{RS}^{ul}}{\partial \omega_k^{ul^2}} = \frac{MN}{\omega_k^{ul^2}\log(2)}, \ \frac{\partial^2 L_{RS}^{ul}}{\partial \omega_k^{ul}\partial \alpha} = -\frac{MN\psi_k T}{\log(2)} \tag{68}$$

$$\frac{\partial^2 L_{RS}}{\partial \omega_k^{ul}\partial \psi_k} = \frac{MN\alpha T}{\log(2)} \tag{69}$$

The Hermitian matrix for the UL time and weight resource allocation problem Lagrangian is represented as

$$\begin{bmatrix} & \alpha & \psi_k & \omega_k^{ul} \\ \alpha & + & - & - \\ \psi_k & - & + & + \\ \omega_k^{ul} & - & + & + \end{bmatrix}. \tag{70}$$

From the Hermitian matrix, L_{RS}^{ul} is non-convex with respect to all variables but convex with respect to individual variables. However, the differentials presented considered α and not $(1-\alpha)$ as a variable. If $(1-\alpha)$ is made a variable, then the total problem becomes a concave problem. ■

From the analysis presented above, both the DL and UL time and weight resource problems are concave problems[5]. Hence, the overall time and weight resource allocation problem is concave.

Appendix C
Optimal Time and Weight Resource Allocation Proof

From (29), let $x_k = \frac{\tilde{\alpha}_k\omega_k^{dl}T}{\log(2)}$ and $z_k = \frac{\hat{\alpha}_k\omega_k^{ul}T}{\log(2)}$, where $\tilde{\alpha}_k = \alpha\tau_k$ and $\hat{\alpha}_k = (1-\alpha)\psi_k$. Thus, the optimization problem in (49) can be rewritten as

$$\begin{aligned} \underset{\{\tilde{\alpha}_k\},\{\hat{\alpha}_k\},\omega_k^{dl},\omega_k^{ul}}{\text{minimize}} \quad & \bar{T}_{RS} \\ \text{subject to} \quad & \sum_{k=1}^{K}\tilde{\alpha}_k + \sum_{k=1}^{K}\hat{\alpha}_k = T, \ \omega_k^{dl} \geq 0, \\ & \sum_{m=1}^{M}\sum_{n=1}^{N}P_{m,n,k}^{ul} \leq P_k^{ul} - P_c, \ \omega_k^{ul} \geq 0 \end{aligned} \tag{71}$$

where

$$\bar{T}_{RS} = \frac{MN}{2}\sum_{k=1}^{K}[x_k - \log_2(x_k)] + MN\sum_{k=1}^{K}[z_k - \log_2(z_k)]. \tag{72}$$

From $\bar{T}_{RS}$ the optimal values of x_k and z_k can be found individually by a line search method using

$$\bar{T}_{RS,k}^{dl} = \frac{MN}{2}[x_k - \log_2(x_k)] \tag{73}$$

[5]The objective functions are individually concave with respect to all the variables. However, the time constraint is linear with respect to all variables. The power constraint is also linear with respect to τ_k and ψ_k, but concave with respect to α. Since the objective function is concave with respect to all variables, both optimization problems are concave problems. Therefore, the total time and weight allocation problem is concave.

and

$$\bar{T}^{ul}_{RS,k} = MN[z_k - \log_2(z_k)]. \tag{74}$$

This implies that the optimum solution of each UN can be found separately. However, by observing $\bar{T}^{dl}_{RS,k}$ and $\bar{T}^{ul}_{RS,k}$, it can be deduced that the optimal values of x_k and z_k are the same for all UNs, i.e. $x^\star_1 = x^\star_2 = \ldots = x^\star_K = z^\star_1 = z^\star_2 = \ldots = z^\star_K = x^\star$. Therefore, the line search will be performed once. Based on this deduction, the optimal $\tilde{\alpha}_k$, ω^{dl}_k, $\hat{\alpha}_k$, and ω^{ul}_k should satisfy

$$\begin{aligned} &\frac{x^\star \log(2)}{T} = \tilde{\alpha}_1 \omega^{dl}_1, \ \frac{x^\star \log(2)}{T} = \tilde{\alpha}_2 \omega^{dl}_2, \ldots, \\ &\frac{x^\star \log(2)}{T} = \tilde{\alpha}_K \omega^{dl}_K \end{aligned} \tag{75}$$

$$\begin{aligned} &\frac{x^\star \log(2)}{T} = \hat{\alpha}_1 \omega^{ul}_1, \frac{x^\star \log(2)}{T} = \hat{\alpha}_2 \omega^{ul}_2, \ldots, \\ &\frac{x^\star \log(2)}{T} = \hat{\alpha}_K \omega^{ul}_K. \end{aligned} \tag{76}$$

Note that different combinations of values (i.e., $\tilde{\alpha}_k$ and ω^{dl}_k, and $\hat{\alpha}_k$ and ω^{ul}_k) can result in $\frac{x^\star \log(2)}{T}$. Therefore, there is a need to find the optimal values of $\tilde{\alpha}_k$, ω^{dl}_k, $\hat{\alpha}_k$, and ω^{ul}_k. First, let the optimal DL and UL weights be defined as

$$\begin{aligned} &\frac{x^\star \log(2)}{\tilde{\alpha}^\star_1 T} = \omega^{dl^\star}_1, \ \frac{x^\star \log(2)}{\tilde{\alpha}^\star_2 T} = \omega^{dl^\star}_2, \ldots \frac{x^\star \log(2)}{\tilde{\alpha}^\star_K T} = \omega^{dl^\star}_K, \\ &\frac{x^\star \log(2)}{\hat{\alpha}^\star_1 T} = \omega^{ul^\star}_1, \frac{x^\star \log(2)}{\hat{\alpha}^\star_2 T} = \omega^{ul^\star}_2, \ldots, \ \frac{x^\star \log(2)}{\hat{\alpha}^\star_K T} = \omega^{ul^\star}_K. \end{aligned} \tag{77}$$

Next, we find the optimal values of $\tilde{\alpha}_k$ and $\hat{\alpha}_k$. The differential of the optimization problem with respect to $\tilde{\alpha}_k$ and $\hat{\alpha}_k$ are given as

$$\frac{\partial L_{RS}}{\partial \tilde{\alpha}_k} = -\mu + \sum_{m=1}^{M}\sum_{n=1}^{N} |\hat{h}^{dl}_{m,n,k}|^2 P^{dl}_{m,n,k} \sum_{j=1}^{K} \frac{\lambda^{ul}_j \beta_j}{\hat{\alpha}_k} = 0, \tag{78}$$

$$\frac{\partial L_{RS}}{\partial \hat{\alpha}_k} = -\hat{\alpha}_k \mu - \frac{\lambda^{ul}_k \beta_k}{\hat{\alpha}^2_k} \sum_{j=1}^{K} \tilde{\alpha}_j \sum_{m=1}^{M}\sum_{n=1}^{N} |\hat{h}^{dl}_{m,n,j}|^2 P^{dl}_{m,n,j} = 0. \tag{79}$$

Multiplying (78) by $\hat{\alpha}_k$, we have

$$-\hat{\alpha}_k \mu + \hat{\alpha}_k \sum_{m=1}^{M}\sum_{n=1}^{N} |\hat{h}^{dl}_{m,n,k}|^2 P^{dl}_{m,n,k} \sum_{j=1}^{K} \frac{\lambda^{ul}_j \beta_j}{\hat{\alpha}_k} = 0, \tag{80}$$

Summing (79) and (80) for all UNs, we have

$$-\sum_{k=1}^{K} \tilde{\alpha}_k \sum_{m=1}^{M}\sum_{n=1}^{N} |\hat{h}^{dl}_{m,n,k}|^2 P^{dl}_{m,n,k} \sum_{j=1}^{K} \frac{\lambda^{ul}_j \beta_j}{\hat{\alpha}_k} - \mu \sum_{k=1}^{K} \hat{\alpha}_k = 0. \tag{81}$$

and

$$\sum_{k=1}^{K} \hat{\alpha}_k \sum_{m=1}^{M}\sum_{n=1}^{N} |\hat{h}^{dl}_{m,n,k}|^2 P^{dl}_{m,n,k} \sum_{j=1}^{K} \frac{\lambda^{ul}_j \beta_j}{\hat{\alpha}_k} - \mu \sum_{k=1}^{K} \hat{\alpha}_k = 0, \tag{82}$$

Now, subtracting (81) from (82) gives

$$\begin{aligned} &\sum_{k=1}^{K} \hat{\alpha}_k \sum_{m=1}^{M}\sum_{n=1}^{N} |\hat{h}^{dl}_{m,n,k}|^2 P^{dl}_{m,n,k} \sum_{j=1}^{K} \frac{\lambda^{ul}_j \beta_j}{\hat{\alpha}_k} \\ &+ \sum_{k=1}^{K} \tilde{\alpha}_k \sum_{m=1}^{M}\sum_{n=1}^{N} |\hat{h}^{dl}_{m,n,k}|^2 P^{dl}_{m,n,k} \sum_{j=1}^{K} \frac{\lambda^{ul}_j \beta_j}{\hat{\alpha}_k} = 0, \end{aligned} \tag{83}$$

$$\sum_{k=1}^{K} (\hat{\alpha}_k + \tilde{\alpha}_k) \sum_{m=1}^{M}\sum_{n=1}^{N} |\hat{h}^{dl}_{m,n,k}|^2 P^{dl}_{m,n,k} \sum_{j=1}^{K} \frac{\lambda^{ul}_j \beta_j}{\hat{\alpha}_k} = 0, \tag{84}$$

$\sum_{m=1}^{M}\sum_{n=1}^{N} |\hat{h}^{dl}_{m,n,k}|^2 P^{dl}_{m,n,k} \sum_{j=1}^{K} \frac{\lambda^{ul}_j \beta_j}{\hat{\alpha}_k} > 0$, $\forall k$, which implies that $\hat{\alpha}_k + \tilde{\alpha}_k = 0$. Therefore, $\hat{\alpha}_k = -\tilde{\alpha}_k$. Moreover, since both $\hat{\alpha}_k$ and $\tilde{\alpha}_k$ are positive valued variables, $\hat{\alpha}_k = \tilde{\alpha}_k$. This implies that the optimal time allocation coincides with equal time allocation, i.e. $\hat{\alpha}_k = \tilde{\alpha}_k = 1/K$. This also leads to equal weight allocations for all UNs according to (77), i.e. $\omega^{dl}_k = \omega^{ul}_k = \omega_k$. Therefore, the weight of UN$_k$ can be found as $\omega^\star_k = \frac{2x^\star K \log(2)}{T^2}$. ■

Appendix D
Convexity Proof and Solution for the Power Resource Allocation Problem

For the power allocation problem, the Lagrangian can be represented as

$$\begin{aligned} L_{RS} = &\sum_{k=1}^{K}\sum_{m=1}^{M}\sum_{n=1}^{N} \log_2\Big(\frac{\sigma^2_k}{|\hat{h}^{dl}_{m,n,k}|^2 P^{dl}_{m,n,k} + \sigma^2_k}\Big) \\ &+ \sum_{k=1}^{K}\sum_{m=1}^{M}\sum_{n=1}^{N} \log_2\Big(\frac{\sigma^2}{|\hat{h}^{ul}_{m,n,k}|^2 P^{ul}_{m,n,k} + \sigma^2}\Big) \\ &- \sum_{k=1}^{K} \lambda^{ul}_k \Big[\sum_{m=1}^{M}\sum_{n=1}^{N} P^{ul}_{m,n,k} + P_c \\ &- \frac{\alpha\beta_k}{(1-\alpha)\psi_k} \sum_{j=1}^{K} \tau_j \sum_{m=1}^{M}\sum_{n=1}^{N} |\hat{h}^{dl}_{m,n,j}|^2 P^{dl}_{m,n,j} \Big] \\ &- \lambda^{dl}\Big(\sum_{k=1}^{K}\sum_{m=1}^{M}\sum_{n=1}^{N} P^{dl}_{m,n,k} - P^{dl}_{0,max} \Big). \end{aligned} \tag{85}$$

The first derivatives of L_{RS} with respect to $P^{dl}_{m,n,k}$ and $P^{ul}_{m,n,k}$ are given as

$$\begin{aligned} \frac{\partial L_{RS}}{\partial P^{dl}_{m,n,k}} = &-\frac{1}{\log(2)}\Big(\frac{|\hat{h}^{dl}_{m,n,k}|^2}{|\hat{h}^{dl}_{m,n,k}|^2 P^{dl}_{m,n,k} + \sigma^2_k}\Big) - \lambda^{dl} + \\ &\tau_k |\hat{h}^{dl}_{m,n,k}|^2 \sum_{j=1}^{K} \frac{\alpha\beta_j \lambda^{ul}_j}{(1-\alpha)\psi_j} \end{aligned} \tag{86}$$

and

$$\frac{\partial L_{RS}}{\partial P^{ul}_{m,n,k}} = -\frac{1}{\log(2)}\Big(\frac{|\hat{h}^{ul}_{m,n,k}|^2}{|\hat{h}^{ul}_{m,n,k}|^2 P^{ul}_{m,n,k} + \sigma^2}\Big) - \lambda^{ul}_k. \tag{87}$$

Furthermore, the second derivatives of L_{RS} with respect to $P^{dl}_{m,n,k}$ and $P^{ul}_{m,n,k}$ are given as

$$\frac{\partial^2 L_{RS}}{\partial P^{dl^2}_{m,n,k}} = \frac{1}{\log(2)}\Big(\frac{|\hat{h}^{dl}_{m,n,k}|^4}{(|\hat{h}^{dl}_{m,n,k}|^2 P^{dl}_{m,n,k} + \sigma^2_k)^2}\Big), \tag{88}$$

$$\frac{\partial^2 L_{RS}}{\partial P_{m,n,k}^{ul^2}} = \frac{1}{\log(2)}\Big(\frac{|\hat{h}_{m,n,k}^{ul}|^4}{(|\hat{h}_{m,n,k}^{ul}|^2 P_{m,n,k}^{ul} + \sigma^2)^2}\Big) \tag{89}$$

and

$$\frac{\partial^2 L_{RS}}{\partial P_{m,n,k}^{dl} \partial P_{m,n,k}^{ul}} = \frac{\partial^2 L_{RS}}{\partial P_{m,n,k}^{ul} \partial P_{m,n,k}^{dl}} = 0. \tag{90}$$

Hence, the Hermitian matrix for L_{RS} is given as

$$\begin{bmatrix} & P_{m,n,k}^{dl} & P_{m,n,k}^{ul} \\ P_{m,n,k}^{dl} & + & 0 \\ P_{m,n,k}^{ul} & 0 & + \end{bmatrix}. \tag{91}$$

From the above Hermitian matrix and second derivatives, it is obvious that L_{RS} is non-convex with respect to both variables. However, L_{RS} is a convex function considering the variables individually. Therefore, from $\frac{\partial L_{RS}}{\partial P_{m,n,k}^{dl}}$ and $\frac{\partial L_{RS}}{\partial P_{m,n,k}^{ul}}$, the optimal $P_{m,n,k}^{dl}$ and $P_{m,n,k}^{ul}$ are defined as

$$P_{m,n,k}^{dl} = \Big[\frac{1}{\log(2)A} - \frac{\sigma_k^2}{|\hat{h}_{m,n,k}^{dl}|^2}\Big] \tag{92}$$

and

$$P_{m,n,k}^{ul} = \Big[\frac{1}{\lambda_k^{ul}\log(2)} - \frac{\sigma^2}{|\hat{h}_{m,n,k}^{ul}|^2}\Big] \tag{93}$$

with $A = (\lambda^{dl} - \tau_k \sum_{m=1}^{M}\sum_{n=1}^{N}|\hat{h}_{m,n,k}^{dl}|^2 \sum_{j=1}^{K}\frac{\alpha\beta_j\lambda_j^{ul}}{(1-\alpha)\psi_j})$.

An iterative algorithm is used to obtain the optimal $P_{m,n,k}^{dl}$ and $P_{m,n,k}^{ul}$ which minimizes problem (50). The optimal λ^{dl} can be found using the bisection method, while the optimal λ_k^{ul} is acquired as

$$\lambda_k^{ul} = \frac{MN}{\log(2)\Big(B - P_c + \sum_{m=1}^{M}\frac{N\sigma^2}{|\hat{h}_{m,n,k}^{ul}|^2}\Big)} \tag{94}$$

with $B = \frac{\alpha\beta_k}{(1-\alpha)\psi_k}\sum_{j=1}^{K}\tau_j\sum_{m=1}^{M}\sum_{n=1}^{N}|\hat{h}_{m,n,j}^{dl}|^2 P_{m,n,j}^{dl}$. ■

REFERENCES

[1] C. Sexton, Q. Bodinier, A. Farhang, N. Marchetti, F. Bader, and L. A. DaSilva, "Enabling asynchronous machine-type D2D communication using multiple waveforms in 5G," *IEEE Int. of Things J.*, vol. 5, no. 2, pp. 1307–1322, apr 2018.

[2] B. Lim and Y. Ko, "SIR analysis of OFDM and GFDM waveforms with timing offset, CFO, and phase noise," *IEEE Transactions on Wireless Communications*, vol. 16, no. 10, pp. 6979–6990, Oct. 2017.

[3] S. Mahama, Y. J. Harbi, A. G. Burr, and D. Grace, "Design and convergence analysis of an IIC-Based BICM-ID receiver for FBMC-QAM systems," *IEEE Open J. of the Comm. Society*, vol. 1, pp. 563 – 577, May 2020.

[4] G. Wunder *et al.*, "5GNOW: non-orthogonal, asynchronous waveforms for future mobile applications," *IEEE Communications Magazine*, vol. 52, no. 2, pp. 97–105, Feb. 2014.

[5] M. Pischella, R. Zakaria, and D. Le Ruyet, "Resource Block-Level Power Allocation in Asynchronous Multi-Carrier D2D Communications," *IEEE Communications Letters*, vol. 21, no. 4, pp. 813–816, Apr. 2017.

[6] B. Farhang-Boroujeny, "OFDM Versus Filter Bank Multicarrier," *IEEE Signal Processing Magazine*, vol. 28, no. 3, pp. 92–112, May 2011.

[7] R. Zakaria and D. Le Ruyet, "A novel filter-bank multicarrier scheme to mitigate the intrinsic interference: Application to mimo systems," *IEEE Transactions on Wireless Communications*, vol. 11, no. 3, pp. 1112–1123, Mar. 2012.

[8] R. Zakaria and D. L. Ruyet, "Intrinsic interference reduction in a filter bank-based multicarrier using QAM modulation," *Physical Communication*, vol. 11, pp. 15–24, Jun. 2014.

[9] H. Nam, M. Choi, S. Han, C. Kim, S. Choi, and D. Hong, "A new filter-bank multicarrier system with two prototype filters for QAM symbols transmission and reception," *IEEE Trans. Wireless Commun.*, vol. 15, no. 9, pp. 5998–6009, Sep. 2016.

[10] S. M. Oteafy and H. S. Hassanein, "Resilient IoT architectures over dynamic sensor networks with adaptive components," *IEEE Internet Things J.*, vol. 4, no. 2, pp. 474–483, Apr. 2017.

[11] S. Mahama, D. K. P. Asiedu, and K.-J. Lee, "Simultaneous wireless information and power transfer for cooperative relay networks with battery," *IEEE Access*, vol. 5, pp. 13 171–13 178, Jul. 2017.

[12] D. K. P. Asiedu, H. Lee, and K.-J. Lee, "Simultaneous wireless information and power transfer for decode-and-forward multihop relay systems in energy-constrained IoT networks," *IEEE Int. Things J.*, vol. 6, no. 6, pp. 9413–9426, Aug. 2019.

[13] B. Clerckx, R. Zhang, R. Schober, D. W. K. Ng, D. I. Kim, and H. V. Poor, "Fundamentals of Wireless Information and Power Transfer: From RF Energy Harvester Models to Signal and System Designs," *IEEE Journal on Selected Areas in Communications*, vol. 37, no. 1, pp. 4–33, Jan. 2019.

[14] F. Mukhlif, K. A. B. Noordin, A. M. Mansoor, and Z. M. Kasirun, "Green transmission for C-RAN based on SWIPT in 5G: a review," *Wireless Net.*, pp. 1–29, May 2018.

[15] A. Prathima, D. S. Gurjar, H. H. Nguyen, and A. Bhardwaj, "Performance Analysis and Optimization of Bidirectional Overlay Cognitive Radio Networks with Hybrid-SWIPT," *IEEE Transactions on Vehicular Technology*, pp. 1–1, 2020.

[16] M. R. A. Khandaker, C. Masouros, K.-K. Wong, and S. Timotheou, "Secure SWIPT by exploiting constructive interference and artificial noise," *IEEE Transaction on Communication*, vol. 67, no. 2, pp. 1326–1340, Feb. 2019.

[17] S. H. Chae, C. Jeong, and S. H. Lim, "Simultaneous wireless information and power transfer for internet of things sensor networks," *IEEE Int. Things J.*, vol. 5, no. 4, pp. 2829–2843, Aug. 2018.

[18] X. Zhou, R. Zhang, and C. K. Ho, "Wireless information and power transfer in multiuser OFDM systems," *IEEE Trans. Wireless Commun.*, vol. 13, no. 4, pp. 2282–2294, Apr. 2014.

[19] W. Lu, Y. Gong, J. Wu, H. Peng, and J. Hua, "Simultaneous wireless information and power transfer based on joint subcarrier and power allocation in OFDM systems," *IEEE Access*, vol. 5, pp. 2763–2770, Feb. 2017.

[20] Z. Na, X. Li, X. Liu, and Z. Deng, "Subcarrier allocation based simultaneous wireless information and power transfer for multiuser OFDM systems," *EURASIP J. Wireless Commun. Netw.*, vol. 2017, no. 1, p. 148, Sep. 2017.

[21] Z. Na, J. Lv, M. Zhang, B. Peng, M. Xiong, and M. Guan, "GFDM based wireless powered communication for cooperative relay system," *IEEE Access*, vol. 7, pp. 50 971–50 979, Apr. 2019.

[22] Z. Na, J. Lv, F. Jiang, M. Xiong, and N. Zhao, "Joint subcarrier and subsymbol allocation-based simultaneous wireless information and power transfer for multiuser GFDM in IoT," *IEEE Internet Things J*, vol. 6, no. 4, pp. 5999–6006, Aug. 2019.

[23] D. C. Melgarejo, J. M. Moualeu, P. Nardelli, G. Fraidenraich, , and D. B. da Costa, "GFDM-Based cooperative relaying networks with wireless energy harvesting," in *Proc. 16th Int. Symposium on Wireless Commun Systems (ISWCS)*. IEEE, Aug. 2019, pp. 416–421.

[24] Y. J. Harbi and A. G. Burr, "On ISI and ICI cancellation for FBMC/OQAM system using iterative decoding and ML detection," in *Wireless Communications and Networking Conference (WCNC)*, Apr. 2016, pp. 1–6.

[25] S. Mahama, Y. J. Harbi, A. G. Burr, and D. Grace, "Iterative interference cancellation in FBMC-QAM systems," in *Wireless Commun. Net. Conf.*, Apr. 2019, pp. 1–5.

[26] ——, "A non-orthogonal waveform design with iterative detection and decoding for narrowband IoT applications," in *in Proc. European Conf. Net. Commun.*, 2019, pp. 1–5.

[27] J. Kim, Y. Park, S. Weon, J. Jeong, S. Choi, and D. Hong, "A new filter-bank multicarrier system: The linearly processed FBMC system," *IEEE Trans. Wireless Commun.*, vol. 17, no. 7, pp. 4888–4898, Jul. 2018.

[28] M. Bellanger, D. Le Ruyet, D. Roviras, M. Terré, J. Nossek, L. Baltar, Q. Bai, D. Waldhauser, M. Renfors, T. Ihalainen *et al.*, "FBMC physical layer: a primer," *Phydyas*, vol. 25, no. 4, pp. 7–10, 2010.

[29] K. W. Choi, A. A. Aziz, D. Setiawan, N. M. Tran, L. Ginting, and D. I. Kim, "Distributed wireless power transfer system for internet-of-things devices," *IEEE Int. of Things J.*, vol. 5, no. 4, pp. 2657–2671, Aug. 2018.

[30] Y. Dong, M. J. Hossain, and J. Cheng, "Performance of Wireless Powered Amplify and Forward Relaying Over Nakagami-m Fading

Channels With Nonlinear Energy Harvester," *IEEE Communications Letters*, vol. 20, no. 4, pp. 672–675, Apr. 2016.
[31] D. K. P. Asiedu, S. Mahama, C. Song, D. Kim, and K.-J. Lee, "Beamforming and resource allocation for multi-user full-duplex wireless powered communications in IoT networks," *IEEE Int. Things J.*, May 2020.
[32] K. W. Choi and D. I. Kim, "Stochastic optimal control for wireless powered communication networks," *IEEE Trans. Wireless Commun*, vol. 15, no. 1, pp. 686–698, Jan. 2016.
[33] E. K. Chong and S. H. Zak, *An introduction to optimization*. John Wiley & Sons, Inc., 2013.
[34] GSMA, "5G, The Internet of Things and Wearablle Devices: Radio Frequency Exposure," GSMA, Tech. Rep., 2019.
[35] Z. Wang, L. Mei, X. Wang, and N. Zhang, "Bit error rate analysis of generalised frequency division multiplexing with weighted-type fractional fourier transform precoding," *IET Commun.*, vol. 11, no. 6, pp. 916–924, Mar. 2017.

Sumaila Mahama (S'17) received the B.Sc. degree in Telecommunications Engineering from the Kwame Nkrumah University of Science and Technology, Ghana, in 2013, the M.S. degree in Electronic Engineering from Hanbat National University, South Korea, in 2016. During 2017, he was with the Department of Electrical and Electronic Engineering, KAAF University College, Ghana, as an assistant lecturer. He worked as a visiting researcher at NEC Laboratories Europe, Heidelberg Germany, in 2019. He is currently pursuing the Ph.D. degree at the Department of Electronic Engineering, University of York, United Kingdom (UK). His Ph.D. research is part of the EU sponsored H2020 MSCA SPOTLIGHT project. His research interests are in wireless communications, particularly, relaying networks, interference cancellation techniques in multi-carrier waveforms and wireless-powered communication networks.

Derek Kwaku Pobi Asiedu (S'17-M'19) acquired his B.Sc in Biomedical Engineering at the University of Ghana (UG), Ghana, in 2011. At the University of Ghana, he completed his coursework for an M.S. in Computer Engineering at the Department of Computer Engineering, UG, in 2017. He received his M.Sc. and Ph.D. in Electronic Engineering at Hanbat National University, South Korea. He was a postdoctoral research fellow at the Communication and Signal Processing Laboratory, Hanbat National University (HBNU), South Korea, in 2019. His current research interests include; wireless information and powered transfer applications in internet-of-things networks, massive MIMO and full-duplex wireless communication, machine learning applications in wireless communication, physical layer security, and biomedical signal processing.

Yahya J. Harbi received B.Sc. and M.Sc. degrees in Electrical Engineering from the University of Baghdad, Iraq, in 2000 and 2002 respectively. In 2017, he received the Ph.D. degree in Electronics Engineering from the University of York, UK. He has been a Lecturer with the University of Kufa, Iraq, since 2004. His research interests are in wireless systems, iterative technique, MIMO and massive MIMO systems.

Kyoung-Jae Lee (S'06–M'11-SM'20) received the B.S., M.S., and Ph.D. degrees from the School of Electrical Engineering, Korea University, Seoul, South Korea, in 2005, 2007, and 2011, respectively. In 2006, he interned with Beceem Communications, Inc., Santa Clara, CA, USA, and in 2009, he visited the University of Southern California, Los Angeles, CA, USA, as a Visiting Student. He was a Research Professor with Korea University in 2011. From 2011 to 2012, he was a Postdoctoral Fellow with the Wireless Networking and Communications Group, University of Texas at Austin, Austin, TX, USA. Since 2012, he has been with the Department of Electronics and Control Engineering, Hanbat National University, Daejeon, South Korea, where he is currently a Professor. In 2020, he was a Visiting Professor with the University of Southern California. His research interests include communication theory, signal processing, and information theory applied to the next-generation wireless communications. He was a recipient of the Best Paper Award at IEEE VTC Fall in 2009, the IEEE ComSoc APB Outstanding Paper Award in 2013, and the IEEE ComSoc APB Outstanding Young Researcher in 2013.

David Grace (S'95-A'99-M'00-SM'13) received his PhD from University of York in 1999, with the subject of his thesis being 'Distributed Dynamic Channel Assignment for the Wireless Environment'. Since 1994 he has been a member of the Department of Electronic Engineering at York, where he is now Professor (Research), Head of Communication Technologies Research Group, and Director of the Centre for High Altitude Platform Applications. Current research interests include aerial platform-based communications, application of artificial intelligence to wireless communications; 5G system architectures; dynamic spectrum access and interference management. He is currently a lead investigator on H2020 MCSA SPOTLIGHT, UK Government funded MANY, dealing with 5G trials in rural areas, and HiQ investigating Quantum Key Distribution from high altitude platforms. He was technical lead on the 14-partner FP6 CAPANINA project that dealt with broadband communications from high altitude platforms. He is an author of over 280 papers, and author/editor of 2 books. He is the former chair of IEEE Technical Committee on Cognitive Networks for the period 2013/4. He is a founding member of the IEEE Technical Committee on Green Communications and Computing. In 2000, he jointly founded SkyLARC Technologies Ltd, and was one of its directors.

Alister G. Burr (Senior Member, IEEE) was born in London, U.K, in 1957. He received the BSc degree in Electronic Engineering from the University of Southampton, U.K in 1979 and the PhD from the University of Bristol in 1984. Between 1975 and 1985 he worked at Thorn-EMI Central Research Laboratories in London. In 1985 he joined the Department of Electronics (now Electronic Engineering) at the University of York, U.K, where he has been Professor of Communications since 2000. His research interests are in wireless communication systems, especially MIMO, cooperative systems, physical layer network coding, and iterative detection and decoding techniques. He has published around 250 papers in refereed international conferences and journals, and is the author of "Modulation and Coding for Wireless Communications" (published by Prentice-Hall/PHEI), and co-author of "Wireless Physical-Layer Network Coding (Cambridge University Press, 2018). In 1999 he was awarded a Senior Research Fellowship by the U.K. Royal Society, and in 2002 he received the J. Langham Thompson Premium from the Institution of Electrical Engineers. He has also given more than 15 invited presentations, including three keynote presentations. He was chair, working group 2, of a series of European COST programmes including IC1004 "Cooperative Radio Communications for Green Smart Environments", and has also served as Associate Editor for IEEE Communications Letters, Workshops Chair for IEEE ICC 2016, and TPC co-chair for PIMRC 2018 and 2020.